

MuscleMap: Towards Video-based Activated Muscle Group Estimation

Kunyu Peng¹, David Schneider¹, Alina Roitberg¹, Kailun Yang^{2,*},
Jiaming Zhang¹, M. Saquib Sarfraz^{1,3}, Rainer Stiefelhagen¹

¹Karlsruhe Institute of Technology, ²Hunan University, ³Mercedes-Benz Tech Innovation

Abstract

In this paper, we tackle the new task of video-based Activated Muscle Group Estimation (AMGE) aiming at identifying currently activated muscular regions of humans performing a specific activity. Video-based AMGE is an important yet overlooked problem. To this intent, we provide the MuscleMap136 featuring >15K video clips with 136 different activities and 20 labeled muscle groups. This dataset opens the vistas to multiple video-based applications in sports and rehabilitation medicine. We further complement the main MuscleMap136 dataset, which specifically targets physical exercise, with Muscle-UCF90 and Muscle-HMDB41, which are new variants of the well-known activity recognition benchmarks extended with AMGE annotations. With MuscleMap136, we discover limitations of state-of-the-art architectures for human activity recognition when dealing with multi-label muscle annotations and good generalization to unseen activities is required. To address this, we propose a new multimodal transformer-based model, TRANSM³E, which surpasses current activity recognition models for AMGE, especially as it comes to dealing with previously unseen activities. ¹

1. Introduction

Knowing which skeletal muscles of the human body are activated benefits sport and rehabilitation medicine from multiple perspectives and prevents inappropriate muscle usage which may cause physical injuries [100]. In health care, patients need to know how to conduct the exercise correctly to recover from surgery [103, 21, 4, 83, 88] or specific diseases [129, 26], e.g., COVID-19 [91, 14]. Knowledge about muscle activations allows for user-centric fitness applications providing insights for everyday users or professional athletes which need specially adapted training. The majority of existing work on Activated Muscle Group Estimation (AMGE) is based on wearable devices with electrode sen-

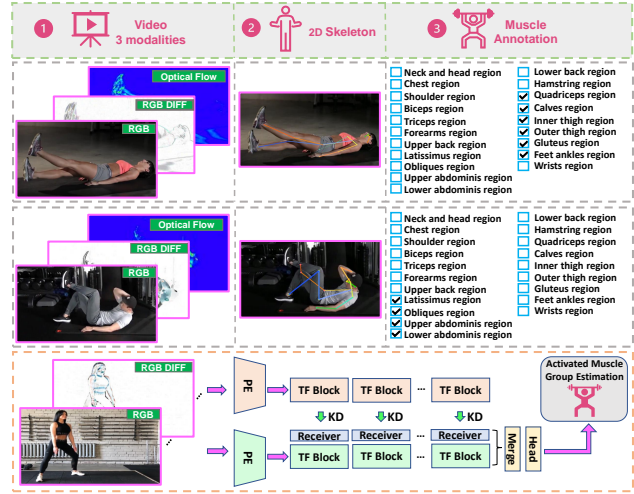


Figure 1: Overview of the proposed MuscleMap136 dataset (Top) and the TRANSM³E model (Bottom). We make use of four data modalities, *i.e.*, RGB, RGB difference (RGB Diff), optical flow, and 2D skeleton. PE and TF denote patch embedding layer and the transformer, respectively.

sors [57, 30, 31, 27, 68, 11]. Yet, many wearable devices are inconvenient and heavy [109, 102], oftentimes used incorrectly [95], and might even cause unnecessary anxiety to the users [24]. A big strength of wearable devices is the high accuracy achieved through direct signal measurement from skin or muscle tissue. However, such exact bio-electrical changes are not required in a large number of medical recovery programs, and knowing the binary activation status of the muscle as shown in Figure 1 is sufficient in many situations [137, 106, 81]. Applying video-based AMGE on smart phones or other widely available smart devices would allow for application of such programs even without access to specialized hardware.

Can modern deep learning algorithms relate fine-grained physical movements to individual muscles? To answer this question, we tackle the new task of video-based AMGE, which estimates muscle contraction during physical activities from video recordings. As there is no previous work for video-based AMGE, we created MuscleMap136 - a video-based dataset with 136 different exercises col-

*Corresponding author (e-mail: kailun.yang@hnu.edu.cn).

¹The datasets and code will be publicly available at <https://github.com/KPeng9510/MuscleMap>.

Table 1: A comparison among the statistics of the video-based datasets, where AR, AQA and CE indicate activity recognition, activity quality assessment, and calorie consumption estimation.

Dataset	NumClips	Task	MultiLabel	NumActions
KTH [61]	599	AR	False	6
UCF101 [117]	13,320	AR	False	101
HMDB51 [67]	6,849	AR	False	51
ActivityNet [16]	28,108	AR	False	200
Kinetics400 [16]	429,256	AR	False	400
Video2Burn [97]	9,789	CE	False	72
MTL-AQA [93]	1,412	AQA	True	/
FineDive [142]	3,000	AQA	True	29
FineGym [111]	32,697	AQA	True	530
MuscleMap136 (Ours)	15,007	AMGE	True	136

lected from YouTube, each exercise annotated with one or multiple out of 20 different muscle group activations, as described in Table 1. To investigate AMGE beyond intensive physical exercises, we additionally extend eligible subsets of the commonly used human activity recognition (HAR) benchmarks HMDB51 [67] and UCF101 [117] with the AMGE annotations, we further refer to these annotated subset datasets as Muscle-HMDB41 and Muscle-UCF90. Since there is no comparable work for video-based AMGE, we select various off-the-shelf Convolutional Neural Networks (CNNs) [18, 42], Graph Convolutional Networks (GCNs) [145, 20, 69] and transformer-based architectures [39, 72, 78] for HAR together with statistic methods as baselines but find that these existing methods can be improved when it comes to fine-grained understanding of human body movements or the adaptation of the learned knowledge to unseen activities and exercises at test-time.

To tackle the aforementioned issue, we propose TRANSM³E, a cross modality knowledge distillation (KD) architecture which combines RGB and RGB difference (RGB Diff) via a new transformer-specific KD mechanism during training. In total, we leverage the most competitive performing architecture MViTv2 [72] as backbone and equip it with three essential novel components designed to achieve a better extraction of the underlying cues for AMGE, *i.e.*, *Multi-Classification Tokens* (MCTs) for AMGE, *Multi-Classification Tokens Knowledge Distillation* (MCTKD) and *Multi-Classification Tokens Fusion* (MCTF). MCTs, similar to the structure setting of MCT in [143], but work differently to harvest informative AMGE cues without specific class alignment. Our proposed MuscleMap benchmark describes a multi-label classification problem where each sample might be annotated with one or up to 20 labels. We use MCTs for AMGE by enriching the single classification (cls) token into 20 to build up the base for cross-modality MCTs-level KD. KD [54] is leveraged as a mechanism for cross modality knowledge transfer after each transformer block which enables us to train with multi-modal data but test with RGB data only. This separates us from preceding work which uses KD as a single-modality knowledge transfer mechanism on the final/intermediate

network layers [84, 41, 123, 75, 54] or other multi-modal architectures which make use of redundant networks to extract per-modality features [45, 60, 126, 92]. While the mentioned MCTKD mechanism integrates cross-modal knowledge into our main network with additional MCTs as KD receiver, another contribution, MCTF, merges the receiver MCTs of KD and the MCTs of major modality at the final layer. By combining these three components, TRANSM³E achieves state-of-the-art performances with superior generalizability compared to the tested baselines. In summary, our contributions are listed as following:

- We introduce video-based Activated Muscle Group Estimation (AMGE) with the aim of lowering the threshold of entry to muscle-activation-based health care and sports applications.
- We provide a new benchmark MuscleMap to propel research on the aforementioned task which includes the *MuscleMap136* dataset as well as *Muscle-HMDB41* and *Muscle-UCF90*. We also present a large number of baseline experiments for this benchmark, including CNN-, transformer-, and GCN-based approaches.
- We propose TRANSM³E, targeting at alleviating the generalization issue of HAR approaches towards unseen activities for AMGE. *Multi-classification Tokens* (MCTs), *Multi-Classification Tokens Knowledge Distillation* (MCTKD) and *Multi-Classification Tokens Fusion* (MCTF) are used to formulate TRANSM³E for AMGE, which shows superior generalization capability on unseen activities and provides state-of-the-art results on the MuscleMap benchmark.

2. Related Work

Muscle Group Activation analysis is predominantly performed using electromyographic (EMG) data [141, 122, 57, 30, 31, 27, 68, 11] either with intramuscular (iEMG) or surface EMG sensors (sEMG).

Activity Recognition is a dominating field within visual human motion analysis which was propelled by the advent of Convolutional Neural Networks (CNNs) with 2D-CNNs [62, 115, 44] in combination with recurrent neural networks (RNNs) [34] or different variations of 3D-CNNs [124, 147, 132, 49, 158, 18, 55, 157, 125, 140, 42]. More recently, transformer-based methods advanced over 3D-CNNs especially with advanced pre-training methods and large datasets [8, 87, 12, 72, 155, 39, 121, 72, 77, 78, 133]. Action quality assessment (AQA) [93, 120] and visual calory estimation (VCE) [97] relate to our work since these methods likewise shift the question of research from *what?* to *how?* with the aim of detailed analysis of human motion. Multimodal data is a common strategy, *e.g.*, by combining RGB video with audio [65, 6, 99, 94, 5], poses [29, 28, 101, 107], optical flow [52, 99], or temporal difference

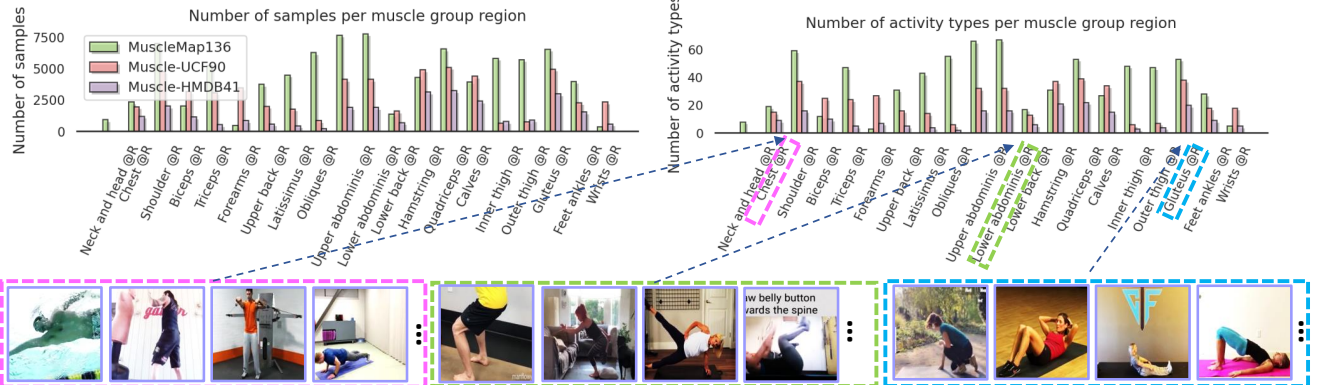


Figure 2: An overview regarding the number of activities and the number of samples per muscle region (@R) for the three datasets depicted at the top. On the bottom some activity-specific samples from MuscleMap136 are shown according to the corresponding muscle group.

images [89]. Body poses are commonly used as a modality for activity recognition on their own. Yan *et al.* [145] and follow-up research [112, 79, 20, 113, 148, 151, 20, 69] make use of GCNs, while competitive approaches leverage CNNs with special pre-processing methods [25, 36].

Knowledge distillation (KD) [54] became a common technique to reduce the size of a neural network while maintaining performance. In review [50], methods can be categorized to focus on knowledge distillation based on final network outputs (response-based) [114, 51, 9, 59, 153], based on intermediate features (feature-based) [74, 159, 152, 146, 58], or based on knowledge about the relations of data samples or features (relation-based) [116, 7, 19, 19]. Recently, adaptations of distillation for transformer architectures gained attraction [1, 138, 75, 70]. Fusion strategies can be grouped into feature-fusion [56, 161, 82, 2, 3, 98, 48, 139] and score fusion [131, 130, 2, 160, 64, 90]. Our work integrates into the former by using KD as a mid-fusion mechanism.

Multi-label classification methods allow for assigning more than a single class to a data sample. Common strategies include per-class binary classifiers with adapted loss functions to counter the imbalance problem [10], methods which make use of spatial knowledge [150, 149, 46, 23], methods which make use of knowledge about label relations [37, 135, 156, 22, 118] or methods which are based on word embeddings [104, 76, 144].

Datasets which combine visual data of the human body with muscle activation information are sparse and mainly limited to specific sub-regions of the human body, *e.g.*, for hand gesture recognition [47]. In contrast, a large variety of full-body HAR datasets were collected in recent years, which are labelled with high-level human activities [67, 117, 63, 110, 73, 96], fine grained human action segments [66, 119, 154, 71], or action quality annotations [111, 142, 93, 120]. We leverage such datasets by extending them with muscle group activation labels.

3. Benchmark

The MuscleMap benchmark consists of three different datasets, each highlighting different strengths of an AMGE approach. While *MuscleMap136* provides a high quality dataset with well-defined muscle activations, *Muscle-HMDB41* and *Muscle-UCF90* present a much harder setting with activities which are more common in everyday living situations. The selected activities in MuscleMap136 as well as in Muscle-HMDB41 and Muscle-UCF90 are specifically chosen based on fitness and health care related resources which are leveraged to derive annotations for them. For each dataset, we provide an evaluation protocol which differentiates between seen and unseen activities.

MuscleMap136. With the new video-based AMGE task in mind, we collect MuscleMap136 by querying YouTube for physical exercise video series. The collected dataset contains 136 activity types as well as 15,007 video clips and is competitive compared to other video-based datasets targeting fine-grained tasks, as shown in Table 1. 20 activities are reserved for the splits of unseen activities.

MuscleMap136 targets physical exercise videos from fitness enthusiasts. Exercises are well suited for AMGE, since they display a large range of motions which are designed to activate specific muscle groups and instructional videos provide high quality examples of the displayed motion. These videos are mostly near-person, which results in a better AMGE understanding. In contrast, Muscle-HMDB41 and Muscle-UCF90 provide a much harder but more diverse setting with many activities which relate to everyday living tasks. Compared with Muscle-UCF90 and Muscle-HMDB41, the MuscleMap136 dataset has more samples and activities per muscle region, especially for the head-and neck region. Statistics regarding the number of samples and the number of activities per muscle region are shown in Figure 2. Our dataset also contains samples with rotated/unrotated camera, varying background, varying gender, body occlusion and varying age to introduce various

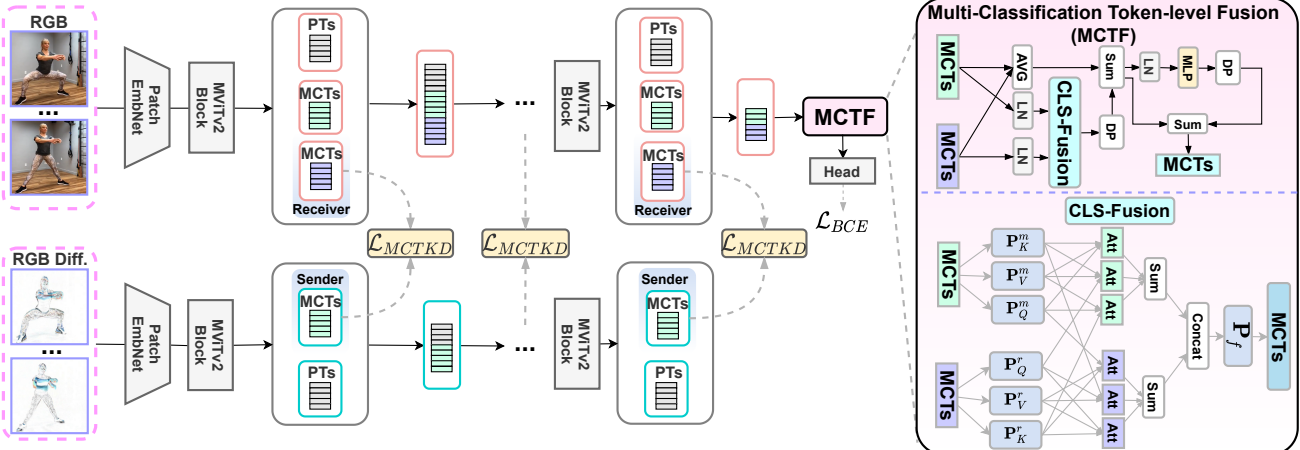


Figure 3: **TRANSM³E**. The knowledge is distilled from the RGB Difference (Diff.) to the RGB, PTs denotes the patch embedding tokens. Three main components are shown, *e.g.*, Multi-Classification Tokens (MCTs), Multi-Classification Tokens Knowledge Distillation (MCTKD), and Multi-Classification Tokens Fusion (MCTF).

domain shift. While RGB video data can be retrieved either by downloading the respective YouTube videos for MuscleMap136 or the original HMDB51 and UCF101 datasets, we also provide optical flow which we calculated using the work of [134] as well as 2D skeleton data which we extracted based on the work of [40], RGB difference data can be efficiently calculated during training. A small set of activities from MuscleMap136 is shown in the bottom part of Figure 2 for the selected muscle region. In Table 1, MuscleMap136 is compared with existing HAR, action quality assessment and calorie consumption datasets. Further details as well as the definition of seen and unseen activity splits are listed in the supplementary.

Muscle-UCF90 is created by providing annotations for an eligible subset of activity classes of UCF101 [117]. UCF101 consists of 13,320 video clips which were originally collected from YouTube with large diversity in object appearances, background, view points, and participants. Muscle-UCF90 provides annotations for 10,553 video clips of 90 activities. Nine of these activities are reserved for the splits of unseen activities. Unlike MuscleMap136 designed for AMGE, some actions of UCF and HMDB do not have well-documented muscle activations, *e.g.*, ApplyLipstick. Since our labeling process is based on expert-based sources, we skipped these actions rather than making assumptions about these activations, ourselves.

Muscle-HMDB41 contains 41 annotated activities with 5,259 samples. Six of these 41 activities are reserved for the splits of unseen activities. Muscle-HMDB41 is a subset of the well-known activity recognition dataset HMDB51 [67] which contains 51 activities with 6,849 video clips. HMDB51 is based on commercial movies and contains scenarios from everyday living scenarios but also depictions of very uncommon situations and environments.

Muscle group annotations. We cluster skeletal muscles into 20 major muscle groups with binary activation as

shown in the checkboxes in Figure 1. As web resource has already tried to be well employed to serve as annotation [93], the pairing of muscle group activations to activities is obtained by statistical majority voting following ImageNet1K [32] on muscle activation descriptions of more than >400 health care and fitness online resources written and reported by well-established coaches, recognized as experts, and including various scientific researches, *e.g.*, [33, 38, 53, 127, 86, 15, 17], where the recorded major activated muscles are used as annotation. To maintain precise AMGE labels, we differentiate between low- and high-level actions as well as different low-level actions of the same category. More details regarding the annotation as well as the exact pairings of muscle groups to activities of MuscleMap136, Muscle-HMDB41 and Muscle-UCF90 are provided in the supplementary.

4. Architecture

Preliminaries of MViT. TRANSM³E is based on the improved multi-scale visual transformer (MViTv2) [72], which is itself based on MViTv1 [39]. Compared with ViT [35], MViTv1 increases the channel resolution progressively and reduces the resolution on the spatiotemporal plane simultaneously, which realizes pooling operations both on Keys (K) and Queries (Q). The basic idea of MViTv1 is the construction of different low- and high-level visual modeling stages [39]. Multi-scale pooling attention is one of the major components of MViTv2 compared with ViT. MViTv2 uses decomposed relative position embeddings and residual pooling connections to integrate the principle of shift-invariance into the model and reduce computational complexity, while the downscaling in MViTv1 is achieved by large strides on the Keys (K) and Values (V).

MCTs. MCTs, which has similar structure with MCT designed for semantic segmentation [143], are used differ-

ently to harvest more informative components to achieve good generalizability for AMGE and to construct sender and receiver for cross-modality KD in our work. The major difference between our AMGE-specific MCTs and the semantic segmentation-specific MCT in [143] is that Xu *et al.* [143] used the MCT outputs from different-stage attention maps and leveraged pooling among channel dimension of each token in MCT to calculate the semantic segmentation map while we directly use the final layer output of MCTs and aggregate the MCTs along token dimension together with Softmax to achieve multi-label classification. Assuming the classification (cls) tokens of MCTs to be referred to by $\text{cls}_j, j \in \{1 \dots C\}$ and the flattened patch embeddings to be referred to as $\{\mathbf{p}_i\}, i \in (1, N_{\text{Patches}})$ for the given input video, where N_{Patches} is the length of the patch sequence, the input of the first MViTv2 block is $\{\text{cls}_1, \text{cls}_2, \dots, \text{cls}_C, \mathbf{p}_1, \dots, \mathbf{p}_{N_{\text{Patches}}}\}$. The final classification is computed through $\text{Output} = \text{Softmax}(\mathbf{P}_\alpha(\sum_{i=1}^C \text{cls}_i / N), \text{dim} = -1)$, where \mathbf{P}_α indicates a fully connected (FC) layer projecting the merged MCTs to a single vector with the number of muscle regions as dimensionality. This final calculation also demonstrates the difference between our AMGE-specific MCTs and the MCT from [143].

MCTKD. Multi-Classification Tokens Knowledge Distillation (MCTKD) is one of our main contributions and to the best of our knowledge we are the first to introduce this technique. Most existing multimodal fusion (MMF) approaches tend to repeat the feature extraction backbone several times [45, 60, 126], resulting in large memory consumption and limited inference speed. This problem increases if a complementary modality has to be calculated at inference time, as can be the case with optical flow or body pose estimation.

In the past, transformer-based KD mainly focused on using intermediate full patch embeddings [84, 75, 41] or final cls token [123], while we propose KD on MCTs for both intermediate and final layers with an additional MCT-based knowledge receiver. The underlying benefit of MCTKD is that the token number of the MCTs is fixed, while KD on patch embeddings [75, 41] may encounter the alignment issue when facing with different modalities with different token size of the patch embeddings.

Instead of directly distilling knowledge from the MCTs of an auxiliary modality towards the MCTs of a major modality, another N cls tokens (Receiver MCTs) are introduced as aforementioned. This approach reduces disturbance of the MCTs for the major modality. Assuming the receiver MCTs of the major modality branch are denoted as $\text{cls}_r = \{\text{cls}_{r,1}, \text{cls}_{r,2}, \dots, \text{cls}_{r,C}\}$ and the sending MCTs from the auxiliary modality branch can be indicated by $\text{cls}_s = \{\text{cls}_{s,1}, \text{cls}_{s,2}, \dots, \text{cls}_{s,C}\}$, MCTKD is achieved by applying KL-Divergence (KL-Div) loss after

each MViTv2 block on cls_r and cls_s :

$$L_{\text{MCTKD},\text{all}} = \left(\sum_{i=1}^{N_B} \text{KL-Div}(\text{cls}_r^i, \text{cls}_s^i) \right) / N_B, \quad (1)$$

where N_B refers to the number of transformer blocks and $L_{\text{MCTKD},\text{all}}$ refers to the sum of all MCTKD losses. $L_{\text{MCTKD},\text{all}}$ is combined equally with the binary cross entropy loss (L_{BCE}).

MCTF. Another major component of TRANSM³E is Multi-Classification Tokens Fusion (MCTF) designed to fuse knowledge receiver MCTs and the original MCTs of the major modality branch, the process is also depicted in Figure 3. Assuming cls_r denotes the receiver MCTs, and cls_m denotes the MCTs from the major modality branch, \mathbf{K} , \mathbf{Q} , and \mathbf{V} for each MCTs can be obtained through linear projections:

$$\begin{aligned} \mathbf{K}_m, \mathbf{Q}_m, \mathbf{V}_m &= \mathbf{P}_K^m(\text{cls}_m), \mathbf{P}_Q^m(\text{cls}_m), \mathbf{P}_V^m(\text{cls}_m), \\ \mathbf{K}_r, \mathbf{Q}_r, \mathbf{V}_r &= \mathbf{P}_K^r(\text{cls}_r), \mathbf{P}_Q^r(\text{cls}_r), \mathbf{P}_V^r(\text{cls}_r). \end{aligned} \quad (2)$$

After obtaining the \mathbf{Q} , \mathbf{K} , and \mathbf{V} from the original and receiver MCTs of the major modality branch, a mixed attention mechanism is calculated as following,

$$\begin{aligned} \mathbf{A}_{mm}^m &= \mathbf{P}_{mm}(DP(\text{Att}(\mathbf{Q}_m, \mathbf{K}_m, \mathbf{V}_m))), \\ \mathbf{A}_{mr}^m &= \mathbf{P}_{mr}(DP(\text{Att}(\mathbf{Q}_m, \mathbf{K}_r, \mathbf{V}_m))), \\ \mathbf{A}_{rm}^m &= \mathbf{P}_{rm}(DP(\text{Att}(\mathbf{Q}_r, \mathbf{K}_m, \mathbf{V}_m))), \end{aligned} \quad (3)$$

where Att denotes the attention operation computed as $\text{Att}(\mathbf{Q}, \mathbf{K}, \mathbf{V}) = \text{Softmax}(\mathbf{Q} @ \mathbf{K}) * \mathbf{V}$ and DP indicates Dropout. The above three equations provide attentions considering different focus perspectives including self-attention \mathbf{A}_{mm}^m and two types of cross attention, *i.e.* \mathbf{A}_{rm}^m and \mathbf{A}_{mr}^m which use the Queries from the original MCTs and the Keys from the receiver MCTs and vice versa. The same procedure is conducted for the receiver MCTs to generate \mathbf{A}_{rr}^r , \mathbf{A}_{rm}^r , and \mathbf{A}_{mr}^r with Dropout denoted by DP through,

$$\begin{aligned} \mathbf{A}_{rr}^r &= \mathbf{P}_{rr}(DP(\text{Att}(\mathbf{Q}_r, \mathbf{K}_r, \mathbf{V}_r))), \\ \mathbf{A}_{rm}^r &= \mathbf{P}_{rm}(DP(\text{Att}(\mathbf{Q}_r, \mathbf{K}_m, \mathbf{V}_r))), \\ \mathbf{A}_{mr}^r &= \mathbf{P}_{mr}(DP(\text{Att}(\mathbf{Q}_m, \mathbf{K}_r, \mathbf{V}_r))). \end{aligned} \quad (4)$$

After the acquisition of different attentions, the attention is finalized as,

$$\begin{aligned} \mathbf{A}_m &= \text{Sum}(\mathbf{A}_{mm}^m, \mathbf{A}_{mr}^m, \mathbf{A}_{rm}^m), \\ \mathbf{A}_r &= \text{Sum}(\mathbf{A}_{rr}^r, \mathbf{A}_{mr}^r, \mathbf{A}_{rm}^r). \end{aligned} \quad (5)$$

The fused attention is thereby calculated through $\mathbf{A}_f = \mathbf{P}_f(\text{Concat}(\mathbf{A}_m, \mathbf{A}_r))$, where \mathbf{P}_f denotes a FC layer. The whole procedure can be indicated by,

$$\mathbf{A}_f = \text{CLS}_f(\text{LN}(\mathbf{cls}_m), \text{LN}(\mathbf{cls}_r)), \quad (6)$$

Table 2: Experimental results on MuscleMap136, Muscle-HMDB41, and Muscle-UCF90. Val_s, val_u, test_s, and test_u denote evaluation sets with seen and unseen activities and test sets with seen and unseen activities, respectively. Val_a and test_a denote the averaged mean average precision (mAP) of seen and unseen activities.

Model	#PM	MuscleMap136 @ mAP						Muscle-UCF90 @ mAP						Muscle-HMDB41 @ mAP					
		Val_s	Val_u	Val_a	Test_s	Test_u	Test_a	Val_s	Val_u	Val_a	Test_s	Test_u	Test_a	Val_s	Val_u	Val_a	Test_s	Test_u	Test_a
Random	0.0M	29.6	28.9	29.3	29.8	28.3	29.1	26.7	22.9	24.8	27.3	22.3	24.8	28.8	16.4	22.6	28.2	17.7	22.9
All Ones	0.0M	29.7	28.3	29.0	29.6	28.0	28.8	26.6	22.2	24.4	26.6	22.0	24.3	27.9	16.1	22.0	27.3	17.1	22.2
All Zeros	0.0M	29.7	28.3	29.0	29.6	28.0	28.8	26.6	22.2	24.4	26.6	22.0	24.3	27.9	16.1	22.0	27.3	17.1	22.2
ST-GCN [145]	2.6M	75.3	56.1	65.7	76.2	53.5	64.9	40.6	52.5	46.6	42.0	51.0	46.5	41.6	34.0	37.8	41.2	37.0	39.1
CTR-GCN [20]	1.4M	60.3	47.3	53.8	57.7	47.3	52.5	40.8	48.9	44.9	41.8	47.7	44.8	30.3	32.9	31.6	29.6	34.1	31.9
HD-GCN [69]	0.8M	71.1	54.3	62.7	70.7	54.2	62.5	35.7	46.3	41.0	35.6	45.2	40.4	40.1	34.0	37.1	40.5	35.7	38.1
C2D (R50) [43]	23.5M	85.5	45.1	65.3	86.2	43.8	65.0	95.8	52.5	74.2	97.5	53.1	75.3	84.8	38.4	61.6	88.8	38.5	63.7
I3D (R50) [18]	20.4M	88.0	47.0	67.5	87.4	46.2	66.8	98.3	51.7	75.0	98.8	53.2	76.0	79.9	37.3	58.6	82.3	37.6	59.9
Slow (R50) [42]	24.3M	93.4	43.6	68.5	94.3	42.4	68.4	96.7	53.7	75.2	96.9	51.2	74.1	82.7	34.7	58.7	85.4	35.2	60.3
SlowFast (R50) [42]	25.3M	94.8	48.1	71.5	96.7	46.9	71.8	91.1	49.8	70.5	92.7	51.6	72.2	76.9	33.3	55.1	78.0	35.0	56.5
MViTv2-S [72]	34.2M	98.5	55.0	77.0	98.8	55.5	77.2	98.6	52.4	75.5	98.5	52.9	75.7	84.9	39.2	62.1	87.7	38.6	63.2
MViTv2-B [72]	51.2M	98.2	57.3	77.8	98.7	56.3	77.5	98.4	52.3	75.4	99.1	50.7	74.9	86.6	38.8	62.7	88.8	41.4	65.1
VideoSwin-S [78]	50.0M	88.0	48.9	68.5	89.1	47.9	68.5	97.9	54.1	76.0	97.9	52.7	75.3	59.9	39.1	49.5	61.4	37.4	49.4
VideoSwin-B [78]	88.0M	90.2	50.3	70.3	90.8	49.7	70.2	98.0	52.8	75.4	98.1	51.2	74.7	65.0	37.1	51.1	67.1	38.4	52.8
TransM ³ E-Small (Ours)	44.4M	99.0	60.6	79.8	99.0	63.4	81.2	98.6	54.3	76.5	99.2	54.6	76.9	88.7	42.0	65.4	89.5	41.4	65.5
TransM ³ E-Base (Ours)	60.7M	99.3	58.4	78.9	99.3	59.7	79.5	98.1	55.0	76.6	98.4	55.1	76.8	88.1	40.7	64.4	90.5	43.5	67.0



Figure 4: Qualitative results for the MViTv2-S [72] and TRANSM³E-Small. GradCam [108] visualization is given, where the cold color region is focused. The ground truth of the selected sample is on the left, the prediction and gradients of the MViTv2, and our approach are shown in the middle and on the right with their predictions.

where LN demonstrates the layer normalization and CLS_f is the CLS-Fusion operation. Assuming we use cls_a to denote the average of major and receiver MCTs by $\text{cls}_a = (\text{cls}_m + \text{cls}_r)/2$, the final fused output is obtained through,

$$\begin{aligned} \text{cls}_f &= \text{cls}_a + \text{CLS}_f(LN(\text{cls}_r), LN(\text{cls}_m)), \\ \text{cls}_f &:= \text{cls}_a + \text{DP}(\mathbf{M}_\theta(LN(\text{cls}_f))), \end{aligned} \quad (7)$$

where \mathbf{M}_θ denotes a multi-layer perception (MLP) based projection and DP denoted dropout operation. MCTKD and MCTF are integrated into the model after N_{MCTs} epochs of training of TRANSM³E with only MCTs for both modalities.

5. Experiments

5.1. Implementation details

All the video-based approaches are pretrained on ImageNet1K [32]. For all experiments we use PyTorch 1.8.0 with 4 V100 GPUs. To achieve the best performance of TRANSM³E, we first train TRANSM³E with only MCTs for both modalities for 40 epochs, and then train TRANSM³E with all components for 10 epochs. We use AdamW [80] with base learning rate (lr) of 0.0001, weight decay of 0.05, momentum of 0.9, and cosine lr scheduler. We used test_u and val_u to test the model on actions excluded from the train set. Test_u and val_u contains actions with unseen muscle activation combinations to test generalization. More details on the evaluation protocol and metrics are provided in the supplementary.

5.2. MuscleMap benchmark

The results of different neural architectures on our MuscleMap136 benchmark are provided in Table 2. As statistics-based baselines we list *Random*, *All Ones*, and *All Zeros* class-wise activated muscle group predictions. The statistic baselines show overall low performances with <30% mAP on all datasets. Skeleton-based approaches, *e.g.*, ST-GCN [145], CTR-GCN [20], and HD-GCN [69], obviously outperform the statistic baselines. Video-based approaches surpass all the others overall, where transformer-based approaches, *e.g.*, MViTv2 S/B [72] and VideoSwin S/B [78], and CNN-based approaches, *e.g.*, C2D [43], I3D [18], Slow [42], SlowFast [42], are leveraged, respectively.

TRANSM³E surpasses all the investigated approaches by large margins by using MCTs, MCTKD, and MCTF. TRANSM³E-SMALL has 79.8%, 81.2%, 76.5%, 76.9%, 65.4%, and 65.5% mAP considering val_a and test_a on MuscleMap136, Muscle-UCF90, and Muscle-HMDB41 datasets, while the performance on unseen activities are mostly highlighted. We also find that the skeleton-based methods, *e.g.*, ST-GCN, CTR-GCN and HD-GCN, do not show comparable results compared with video-based methods, which can be caused by the observance of the important visual cues for AMGE task. On MuscleMap136, TRANSM³E-SMALL outperforms MViTv2-S by 2.8% and 4.0% on the val_a and test_a, which especially works well for val_u and test_u as TRANSM³E-SMALL surpasses MViTv2-S by 5.6% and 7.9%. Consistent improvements are obtained on Muscle-UCF90 and Muscle-HMDB41 datasets.

5.3. Ablation experiments

This section presents ablation experiments on various design decisions of our architecture, all ablation experiments were performed with TRANSM³E-SMALL.

Ablation study of TRANSM³E. The ablation study of

Table 3: Ablation for TransM³E on the MuscleMap136.

MCTs	MCTKD	MCTF	Val_s	Val_u	Val_a	Test_s	Test_u	Test_a
			98.5	55.0	77.0	98.8	55.5	77.2
✓			98.7	58.3	78.5	98.8	61.3	80.1
✓	✓		98.7	60.5	79.6	99.0	62.6	80.8
✓	✓	✓	99.0	60.6	79.8	99.0	63.4	81.2

Table 4: Ablation regarding different KDs for MCTKD on MuscleMap136.

Method	CW	TW	FP	Val_s	Val_u	Val_a	Test_s	Test_u	Test_a
PatchEmbKD	✓			98.5	59.7	79.1	98.9	61.3	80.1
PatchEmbKD		✓		98.5	59.5	79.0	98.7	61.4	80.1
PatchEmbKD			✓	98.7	58.6	78.7	98.9	61.1	80.0
SparseKD	✓			98.3	60.1	79.2	98.5	61.8	80.2
SparseKD		✓		97.9	59.7	78.8	98.3	62.0	80.2
SparseKD			✓	97.9	58.9	78.4	98.1	61.5	79.8
DenseKD	✓			98.9	59.2	79.1	98.9	61.1	63.1
DenseKD		✓		98.8	59.7	79.3	98.9	61.2	63.2
DenseKD			✓	98.5	58.3	78.4	98.7	60.3	79.5
FinalLayerKD	✓			98.5	59.7	79.1	98.9	61.3	80.1
FinalLayerKD		✓		98.7	59.3	79.0	98.4	61.2	79.8
FinalLayerKD			✓	98.7	59.0	78.9	98.9	61.0	80.0
PatchEmbMCTKD (Ours)	✓			98.7	59.5	79.2	98.9	61.4	80.2
PatchEmbMCTKD (Ours)		✓		98.8	59.1	79.0	98.9	61.5	80.2
PatchEmbMCTKD (Ours)			✓	98.6	58.8	78.7	98.9	61.3	80.1
SparseMCTKD (Ours)	✓			98.7	59.4	79.1	98.9	61.2	80.1
SparseMCTKD (Ours)		✓		98.8	58.9	78.9	99.0	61.7	80.4
SparseMCTKD (Ours)			✓	98.6	58.4	78.5	98.9	61.0	80.0
DenseMCTKD (Ours)	✓			98.6	58.3	78.5	98.9	61.1	80.0
DenseMCTKD (Ours)		✓		98.7	60.5	79.6	99.0	62.6	80.8
DenseMCTKD (Ours)			✓	98.4	59.0	78.7	98.7	60.6	79.7
FinalLayerMCTKD (Ours)	✓			98.8	59.0	78.9	98.9	61.2	80.1
FinalLayerMCTKD (Ours)		✓		98.7	58.6	78.7	98.8	61.0	79.9
FinalLayerMCTKD (Ours)			✓	98.9	59.1	79.0	99.0	61.4	80.2

Table 5: Ablation for the MCTF on MuscleMap136.

Method	Val_s	Val_u	Val_a	Test_s	Test_u	Test_a
Sum [105]	98.8	60.4	79.6	99.1	61.9	80.5
Concatenation [105]	98.7	60.5	79.6	99.0	62.6	80.8
Multiplication [105]	98.4	60.1	79.3	98.5	62.3	80.4
SelfAttention [85]	98.5	60.5	79.5	98.9	62.7	80.8
CrossAttention [85]	98.8	59.6	79.2	98.8	62.4	80.6
AttentionBottleNeck [85]	98.7	60.4	79.6	99.0	62.2	80.6
TransM ³ E-Small	99.0	60.6	79.8	99.0	63.4	81.2

Table 6: Comparison among our approach and different MMF/KD on MuscleMap136.

Method	Val_s	Val_u	Val_a	Test_s	Test_u	Test_a
LateFusionSum [105]	98.6	54.2	76.4	98.9	54.8	76.9
LateFusionConcat [136]	70.1	52.0	61.1	71.3	52.1	61.7
LateFusionMul [105]	53.8	35.8	44.8	54.0	35.9	45.0
CrossAttention [85]	83.6	40.7	62.2	87.7	40.6	64.2
PEFusionSum [96]	97.7	56.3	77.0	98.6	56.7	77.7
PEFusionConcat [96]	97.1	51.9	74.5	97.9	49.2	73.6
PEFusionMul [96]	97.7	51.4	74.6	98.1	51.1	74.6
MixedFusion [96]	98.8	52.8	75.8	98.8	52.9	75.9
DeiT [123]	98.2	51.9	75.1	98.8	53.4	76.1
ConventionalKD [54]	68.8	49.7	59.3	67.0	48.2	57.6
Ours	99.0	60.6	79.8	99.0	63.4	81.2

Table 7: Experiments for different modalities on MuscleMap136.

Modality	Val_s	Val_u	Val_a	Test_s	Test_u	Test_a
Optical Flow	69.8	48.8	59.3	63.5	44.0	53.8
RGB Difference	96.1	58.0	77.1	96.5	56.5	76.5
RGB	98.7	60.5	79.6	98.8	61.3	80.1

components, *i.e.*, MCTs, MCTKD, and MCTF, is shown in Table 3. The performance of TRANSM³E-SMALL is increased step by step, while using all three components reaches the best performance.

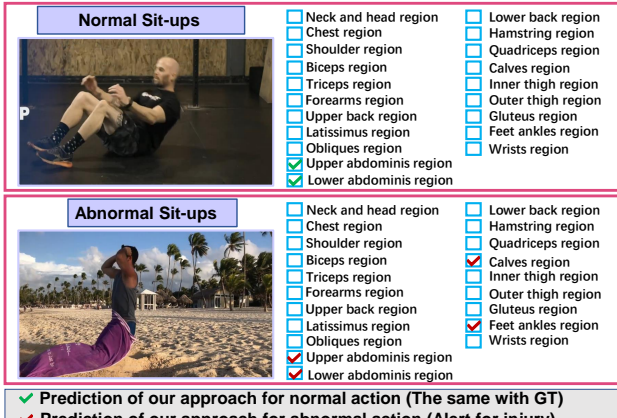


Figure 5: A sample of use case for dangerous behavior alert by abnormal AMGE during human body movement, while AMGE is achieved by TRANSM³E-SMALL.

Selection of modalities We systematically search for the best performing primary and secondary modalities and present the results in Table 7. RGB and RGB Diff present best performances.

Multi-Classification Tokens Knowledge Distillation. In this experiment we ablate KD with or without receiver MCTs and list the results in Table 4. We differentiate between channel-wise (CW), token-wise (TW) and full patch-wise (FP) knowledge distillation. CW means executing Softmax along the channel instead of token dimension (TW). Additionally we evaluate the effects of varying the location of KD application, *i.e.*, at the patch embedding layer (PatchEmbKD/MCTKD), at the final layer (FinalLayerKD/MCTKD), after token size reduction (SparseKD/MCTKD), or after each MViTv2 block (DenseKD/MCTKD). DenseMCTKD (TW) achieves the best performance, thereby it is used to build our MCTKD. The performance of MCTKD (TW) outperforms the second best approaches, *i.e.*, DenseKD (CW) and SparseMCTKD (FP) for val_a and test_a, by 0.3% and 0.4% in mAP.

Multi-Classification Tokens Fusion. The ablations on MCTF for TRANSM³E-SMALL are presented in Table 5, where our approach is compared with existing fusion approaches. MCTF shows the best performance with 79.8% and 81.2% on val_a and test_a of MuscleMap136. The superiority of our MCTF compared to other attention-based approaches is based on leveraging attention from a more diverse perspective, which benefits the capability of integration considering different focus formats of the attention.

Multimodal fusion and Knowledge Distillation. Table 6 presents the comparison between TRANSM³E-SMALL and existing MMF and KD approaches, *i.e.*, late fusion (LF) sum, LF multiplication, LF concatenation, patch embedding (PE) sum, PE multiplication, PE concatenation, cross attention, mixed attention, and the KD pipeline in DeiT [123] while using MViTv2-S as backbone. The evaluated MMF-based approaches are mostly two-branch-based, which du-

plicate either the patch embedding network or the whole backbone for feature extraction. Our approach has diverse benefits, *i.e.*, the KD-based fusion barely increases the model complexity during inference, which ensures proper memory usage and fast inference, and the data of the auxiliary modality is only required during training. For example, the number of parameters (#PM) of LF Sum is 68.5M while #PM for the TRANSM³E-SMALL is 44.4M. Additionally, another sensor and data from another modality do not need to be set up or calculated during inference. Adding more complexity for MMF decreases the generalization ability if we focus at val_u and test_u, where LF Sum shows the best performance among MMF. Compared to the best evaluated approach for MMF (LateFusionSum), our approach has 0.4%, 6.4%, 3.4%, 0.1%, 8.6%, and 4.3% mAP improvements for val_s, val_u, val_a, test_s, test_u, and test_a respectively. Our approach also surpasses the DeiT pipeline [123] by a large margin, especially in terms of the generalizability.

5.4. Analysis of qualitative results and use case

Qualitative AMGE results are shown in Figure 4, the ground truth and GradCam [108] visualizations of MViTv2-S and TRANSM³E-SMALL with their predictions are given from left to right. The true/missed/false prediction is marked as green checkmark/purple crossmark/red crossmark. Overall, our approach has more accurate predictions and less false and missed predictions for all the samples considering unseen activities, *i.e.*, sample 1, 2 and 3, and seen activities, *e.g.*, sample 4 and 5, where sample 3, 4, and 5 are fully correctly predicted. Specifically, TRANSM³E-SMALL concentrates mostly on the accurate regions of the human body, *e.g.*, in sample 5 TRANSM³E-SMALL focuses on the leg-related region, which is the dominant region according to its ground truth, while MViTv2-S focuses additionally on the chest and feet regions which results in more false predictions. In sample 4, the abdominal region of the human body is focused correctly by TRANSM³E-SMALL. A further use case is shown in Figure 5, predicting abnormal activity execution. This sample illustrates that our approach can be leveraged to detect abnormal exercise behavior and dangerous muscle usage for health care and sports.

6. Conclusion

In this paper we open the vistas of video-based activated muscle group estimation. We establish the MuscleMap benchmark, with annotation sets for UCF101 and HMDB51 as well as the new MuscleMap136 dataset to facilitate learning-based muscle group estimation. We propose TRANSM³E with multi-classification token distillation and fusion in a cross-modality manner for enhancing the generalization performance on unseen activities. TRANSM³E sets the state-of-the art on all three proposed datasets included in this benchmark.

References

[1] Gustavo Aguilar, Yuan Ling, Yu Zhang, Benjamin Yao, Xing Fan, and Chenlei Guo. Knowledge distillation from internal representations. In *AAAI*, 2020. 3

[2] Zeeshan Ahmad and Naimul Khan. Human action recognition using deep multilevel multimodal (M^2) fusion of depth and inertial sensors. *IEEE Sensors Journal*, 2019. 3

[3] Zeeshan Ahmad and Naimul Khan. CNN-based multistage gated average fusion (MGAF) for human action recognition using depth and inertial sensors. *IEEE Sensors Journal*, 2020. 3

[4] Neelam Ahuja, Kamal Awad, Sara Peper, Marco Brotto, and Venu Varanasi. Mini review: Biomaterials in repair and regeneration of nerve in a volumetric muscle loss. *Neuroscience Letters*, 2021. 1

[5] Jean-Baptiste Alayrac, Adria Recasens, Rosalia Schneider, Relja Arandjelović, Jason Ramapuram, Jeffrey De Fauw, Lucas Smaira, Sander Dieleman, and Andrew Zisserman. Self-supervised multimodal versatile networks. In *NeurIPS*, 2020. 2

[6] Humam Alwassel, Dhruv Mahajan, Bruno Korbar, Lorenzo Torresani, Bernard Ghanem, and Du Tran. Self-supervised learning by cross-modal audio-video clustering. In *NeurIPS*, 2020. 2

[7] Shumin An, Qingmin Liao, Zongqing Lu, and Jing-Hao Xue. Efficient semantic segmentation via self-attention and self-distillation. *T-ITS*, 2022. 3

[8] Anurag Arnab, Mostafa Dehghani, Georg Heigold, Chen Sun, Mario Lučić, and Cordelia Schmid. ViViT: A video vision transformer. In *ICCV*, 2021. 2

[9] Haoli Bai, Hongda Mao, and Dinesh Nair. Dynamically pruning segformer for efficient semantic segmentation. In *ICASSP*, 2022. 3

[10] Emanuel Ben-Baruch, Tal Ridnik, Nadav Zamir, Asaf Noy, Itamar Friedman, Matan Protter, and Lih Zelnik-Manor. Asymmetric loss for multi-label classification. *arXiv preprint arXiv:2009.14119*, 2020. 3

[11] Kelly R. Berckmans, Birgit Castelein, Dorien Borms, Thierry Parlevliet, and Ann Cools. Rehabilitation exercises for dysfunction of the scapula: Exploration of muscle activity using fine-wire EMG. *The American Journal of Sports Medicine*, 2021. 1, 2

[12] Gedas Bertasius, Heng Wang, and Lorenzo Torresani. Is space-time attention all you need for video understanding? In *ICML*, 2021. 2

[13] Lars Buitinck, Gilles Louppe, Mathieu Blondel, Fabian Pedregosa, Andreas Mueller, Olivier Grisel, Vlad Niculae, Peter Prettenhofer, Alexandre Gramfort, Jaques Grobler, Robert Layton, Jake VanderPlas, Arnaud Joly, Brian Holt, and Gaël Varoquaux. API design for machine learning software: experiences from the scikit-learn project. In *ECML PKDD Workshop: Languages for Data Mining and Machine Learning*, 2013. 20

[14] Louise C. Burgess, Lalitha Venugopalan, James Badger, Tamsyn Street, Alon Gad, Jonathan C. Jarvis, Thomas W. Wainwright, Tamara Everington, Paul Taylor, and Ian D. Swain. Effect of neuromuscular electrical stimulation on the recovery of people with COVID-19 admitted to the intensive care unit: A narrative review. *Journal of Rehabilitation Medicine*, 2021. 1

[15] Jeannette M. Byrne, Nicole S. Bishop, Andrew M. Caines, Kalynn A. Crane, Ashley M. Feaver, and Gregory E. P. Pearcey. Effect of using a suspension training system on muscle activation during the performance of a front plank exercise. *The Journal of Strength & Conditioning Research*, 2014. 4

[16] Fabian Caba Heilbron, Victor Escorcia, Bernard Ghanem, and Juan Carlos Niebles. ActivityNet: A large-scale video benchmark for human activity understanding. In *CVPR*, 2015. 2

[17] Felipe P. Carpes, Fernando Diefenthäler, Rodrigo R. Bini, Darren J. Stefanyshyn, Irvin E. Faria, and Carlos B. Mota. Influence of leg preference on bilateral muscle activation during cycling. *Journal of Sports Sciences*, 2011. 4

[18] Joao Carreira and Andrew Zisserman. Quo vadis, action recognition? A new model and the kinetics dataset. In *CVPR*, 2017. 2, 6, 7, 14

[19] Pengguang Chen, Shu Liu, Hengshuang Zhao, and Jiaya Jia. Distilling knowledge via knowledge review. In *CVPR*, 2021. 3

[20] Yuxin Chen, Ziqi Zhang, Chunfeng Yuan, Bing Li, Ying Deng, and Weiming Hu. Channel-wise topology refinement graph convolution for skeleton-based action recognition. In *ICCV*, 2021. 2, 3, 6, 7, 14

[21] Yu-Pin Chen, Yi-Jie Kuo, Shen-Wu Hung, Tsai-wei Wen, Pei-Chun Chien, Ming-Hsiu Chiang, Nicola Maffulli, and Chung-Ying Lin. Loss of skeletal muscle mass can be predicted by sarcopenia and reflects poor functional recovery at one year after surgery for geriatric hip fractures. *Injury*, 2021. 1

[22] Zhao-Min Chen, Xiu-Shen Wei, Peng Wang, and Yanwen Guo. Multi-label image recognition with graph convolutional networks. In *CVPR*, 2019. 3

[23] Xing Cheng, Hezheng Lin, Xiangyu Wu, Dong Shen, Fan Yang, Honglin Liu, and Nian Shi. MITr: Multi-label classification with transformer. In *ICME*, 2022. 3

[24] Avishek Choudhury and Onur Asan. Impact of using wearable devices on psychological distress: Analysis of the health information national trends survey. *International Journal of Medical Informatics*, 2021. 1

[25] Vasileios Choutas, Philippe Weinzaepfel, Jérôme Revaud, and Cordelia Schmid. PoTion: Pose motion representation for action recognition. In *CVPR*, 2018. 3

[26] Michael C. Cox, Matthew Booth, Gabriela Ghita, Zhongkai Wang, Anna Gardner, Russell B. Hawkins, Dijoia B. Darden, Christiaan Leeuwenburgh, Lyle L. Moldawer, Frederick A. Moore, Philip A. Efron, Steven Anton, and Scott C. Brakenridge. The impact of sarcopenia and acute muscle mass loss on long-term outcomes in critically ill patients with intra-abdominal sepsis. *Journal of Cachexia, Sarcopenia and Muscle*, 2021. 1

[27] Martin Eriksson Crommert, Anna Bjerkefors, Olga Tarassova, and Maria M. Ekblom. Abdominal muscle activation during common modifications of the trunk curl-up

exercise. *The Journal of Strength & Conditioning Research*, 2021. 1, 2

[28] Srijan Das, Rui Dai, Di Yang, and Francois Bremond. VPN++: Rethinking video-pose embeddings for understanding activities of daily living. *arXiv preprint arXiv:2105.08141*, 2021. 2

[29] Srijan Das, Saurav Sharma, Rui Dai, Francois Bremond, and Monique Thonnat. VPN: Learning video-pose embedding for activities of daily living. In *ECCV*, 2020. 2

[30] Roberto M. de Freitas, Atsushi Sasaki, Dimitry G. Sayenko, Yohei Masugi, Taishin Nomura, Kimitaka Nakazawa, and Matija Milosevic. Selectivity and excitability of upper-limb muscle activation during cervical transcutaneous spinal cord stimulation in humans. *Journal of Applied Physiology*, 2021. 1, 2

[31] Ajise Willem de Vries, Frank Krause, and Michiel Pieter de Looze. The effectivity of a passive arm support exoskeleton in reducing muscle activation and perceived exertion during plastering activities. *Ergonomics*, 2021. 1, 2

[32] Jia Deng, Wei Dong, Richard Socher, Li-Jia Li, Kai Li, and Li Fei-Fei. ImageNet: A large-scale hierarchical image database. In *CVPR*, 2009. 4, 7

[33] Lindsay J. Distefano, J. Troy Blackburn, Stephen W. Marshall, and Darin A. Padua. Gluteal muscle activation during common therapeutic exercises. *Journal of Orthopaedic & Sports Physical Therapy*, 2009. 4

[34] Jeffrey Donahue, Lisa Anne Hendricks, Sergio Guadarrama, Marcus Rohrbach, Subhashini Venugopalan, Kate Saenko, and Trevor Darrell. Long-term recurrent convolutional networks for visual recognition and description. In *CVPR*, 2015. 2

[35] Alexey Dosovitskiy, Lucas Beyer, Alexander Kolesnikov, Dirk Weissenborn, Xiaohua Zhai, Thomas Unterthiner, Mostafa Dehghani, Matthias Minderer, Georg Heigold, Sylvain Gelly, Jakob Uszkoreit, and Neil Houlsby. An image is worth 16x16 words: Transformers for image recognition at scale. In *ICLR*, 2021. 4

[36] Haodong Duan, Yue Zhao, Kai Chen, Dahua Lin, and Bo Dai. Revisiting skeleton-based action recognition. In *CVPR*, 2022. 3

[37] Thibaut Durand, Nazanin Mehrasa, and Greg Mori. Learning a deep ConvNet for multi-label classification with partial labels. In *CVPR*, 2019. 3

[38] Rafael F Escamilla, Clare Lewis, Duncan Bell, Gwen Bramblett, Jason Daffron, Steve Lambert, Amanda Pecson, Rodney Imamura, Lonnie Paulos, and James R. Andrews. Core muscle activation during Swiss ball and traditional abdominal exercises. *Journal of Orthopaedic & Sports Physical Therapy*, 2010. 4

[39] Haoqi Fan, Bo Xiong, Karttikeya Mangalam, Yanghao Li, Zhicheng Yan, Jitendra Malik, and Christoph Feichtenhofer. Multiscale vision transformers. In *ICCV*, 2021. 2, 4, 14

[40] Hao-Shu Fang, Jiefeng Li, Hongyang Tang, Chao Xu, Haoyi Zhu, Yuliang Xiu, Yong-Lu Li, and Cewu Lu. AlphaPose: Whole-body regional multi-person pose estimation and tracking in real-time. *TPAMI*, 2022. 4

[41] Zhiyuan Fang, Jianfeng Wang, Xiaowei Hu, Lijuan Wang, Yezhou Yang, and Zicheng Liu. Compressing visual-linguistic model via knowledge distillation. In *ICCV*, 2021. 2, 5

[42] Christoph Feichtenhofer, Haoqi Fan, Jitendra Malik, and Kaiming He. SlowFast networks for video recognition. In *ICCV*, 2019. 2, 6, 7, 14, 17, 20

[43] Christoph Feichtenhofer, Axel Pinz, and Richard P Wildes. Spatiotemporal multiplier networks for video action recognition. In *CVPR*, 2017. 6, 7, 14

[44] Christoph Feichtenhofer, Axel Pinz, and Andrew Zisserman. Convolutional two-stream network fusion for video action recognition. In *CVPR*, 2016. 2

[45] Konrad Gadzicki, Razieh Khamsehshari, and Christoph Zetsche. Early vs late fusion in multimodal convolutional neural networks. In *FUSION*, 2020. 2, 5

[46] Bin-Bin Gao and Hong-Yu Zhou. Learning to discover multi-class attentional regions for multi-label image recognition. *TIP*, 2021. 3

[47] Qing Gao, Jinguo Liu, and Zhaojie Ju. Hand gesture recognition using multimodal data fusion and multiscale parallel convolutional neural network for human–robot interaction. *Expert Systems*, 2021. 3

[48] Ruohan Gao, Tae-Hyun Oh, Kristen Grauman, and Lorenzo Torresani. Listen to look: Action recognition by previewing audio. In *CVPR*, 2020. 3

[49] Rohit Girdhar, Deva Ramanan, Abhinav Gupta, Josef Sivic, and Bryan Russell. ActionVLAD: Learning spatio-temporal aggregation for action classification. In *CVPR*, 2017. 2

[50] Jianping Gou, Baosheng Yu, Stephen J. Maybank, and Dacheng Tao. Knowledge distillation: A survey. *IJCV*, 2021. 3

[51] Qiushan Guo, Xinjiang Wang, Yichao Wu, Zhipeng Yu, Ding Liang, Xiaolin Hu, and Ping Luo. Online knowledge distillation via collaborative learning. In *CVPR*, 2020. 3

[52] Tengda Han, Weidi Xie, and Andrew Zisserman. Self-supervised co-training for video representation learning. In *NeurIPS*, 2020. 2

[53] Dustin H. Hardwick, Justin A. Beebe, Mary Kate McDonnell, and Catherine E. Lang. A comparison of serratus anterior muscle activation during a wall slide exercise and other traditional exercises. *Journal of Orthopaedic & Sports Physical Therapy*, 2006. 4

[54] Geoffrey E. Hinton, Oriol Vinyals, and Jeffrey Dean. Distilling the knowledge in a neural network. *arXiv preprint arXiv:1503.02531*, 2015. 2, 3, 7

[55] Andrew G Howard, Menglong Zhu, Bo Chen, Dmitry Kalenichenko, Weijun Wang, Tobias Weyand, Marco Andreetto, and Hartwig Adam. MobileNets: Efficient convolutional neural networks for mobile vision applications. *arXiv preprint arXiv:1704.04861*, 2017. 2

[56] Javed Imran and Balasubramanian Raman. Evaluating fusion of RGB-D and inertial sensors for multimodal human action recognition. *JAIHC*, 2020. 3

[57] Woohyoung Jeon, Jill Whitall, Lisa Griffin, and Kelly P. Westlake. Trunk kinematics and muscle activation patterns

during stand-to-sit movement and the relationship with postural stability in aging. *Gait & Posture*, 2021. 1, 2

[58] Deyi Ji, Haoran Wang, Mingyuan Tao, Jianqiang Huang, Xian-Sheng Hua, and Hongtao Lu. Structural and statistical texture knowledge distillation for semantic segmentation. In *CVPR*, 2022. 3

[59] Xiao Jin, Baoyun Peng, Yichao Wu, Yu Liu, Jiaheng Liu, Ding Liang, Junjie Yan, and Xiaolin Hu. Knowledge distillation via route constrained optimization. In *ICCV*, 2019. 3

[60] Hamid Reza Vaezi Joze, Amirreza Shaban, Michael L. Iuzzolino, and Kazuhito Koishida. MMTM: Multimodal transfer module for CNN fusion. In *CVPR*, 2020. 2, 5

[61] Soo Min Kang and Richard P. Wildes. Review of action recognition and detection methods. *arXiv preprint arXiv:1610.06906*, 2016. 2

[62] Andrej Karpathy, George Toderici, Sanketh Shetty, Thomas Leung, Rahul Sukthankar, and Li Fei-Fei. Large-scale video classification with convolutional neural networks. In *CVPR*, 2014. 2

[63] Will Kay, João Carreira, Karen Simonyan, Brian Zhang, Chloe Hillier, Sudheendra Vijayanarasimhan, Fabio Viola, Tim Green, Trevor Back, Paul Natsev, Mustafa Suleyman, and Andrew Zisserman. The kinetics human action video dataset. *arXiv preprint arXiv:1705.06950*, 2017. 3

[64] Evangelos Kazakos, Arsha Nagrani, Andrew Zisserman, and Dima Damen. EPIC-fusion: Audio-visual temporal binding for egocentric action recognition. In *ICCV*, 2019. 3

[65] Bruno Korbar, Du Tran, and Lorenzo Torresani. Co-operative learning of audio and video models from self-supervised synchronization. In *NeurIPS*, 2018. 2

[66] Hilde Kuehne, Ali Bilgin Arslan, and Thomas Serre. The language of actions: Recovering the syntax and semantics of goal-directed human activities. In *CVPR*, 2014. 3

[67] Hildegard Kuehne, Hueihan Jhuang, Estíbaliz Garrote, Tomaso Poggio, and Thomas Serre. HMDB: A large video database for human motion recognition. In *ICCV*, 2011. 2, 3, 4, 14

[68] Luciana Labanca, Massimiliano Mosca, Marco Ghislieri, Valentina Agostini, Marco Knaflitz, and Maria Grazia Benedetti. Muscle activations during functional tasks in individuals with chronic ankle instability: a systematic review of electromyographical studies. *Gait & Posture*, 2021. 1, 2

[69] Jungho Lee, Minhyeok Lee, Dogyoon Lee, and Sangyoon Lee. Hierarchically decomposed graph convolutional networks for skeleton-based action recognition. *arXiv preprint arXiv:2208.10741*, 2022. 2, 3, 6, 7, 14

[70] Yeonghyeon Lee, Kangwook Jang, Jahyun Goo, Youngmoon Jung, and Hoirin Kim. FitHuBERT: Going thinner and deeper for knowledge distillation of speech self-supervised learning. *arXiv preprint arXiv:2207.00555*, 2022. 3

[71] Ang Li, Meghana Thotakuri, David A. Ross, João Carreira, Alexander Vostrikov, and Andrew Zisserman. The AVA-kinetics localized human actions video dataset. *arXiv preprint arXiv:2005.00214*, 2020. 3

[72] Yanghao Li, Chao-Yuan Wu, Haoqi Fan, Karttikeya Mangalam, Bo Xiong, Jitendra Malik, and Christoph Feichtenhofer. MViTv2: Improved multiscale vision transformers for classification and detection. In *CVPR*, 2022. 2, 4, 6, 7, 14, 15, 17, 19

[73] Jun Liu, Amir Shahroudy, Mauricio Perez, Gang Wang, Ling-Yu Duan, and Alex C Kot. NTU RGB+D 120: A large-scale benchmark for 3D human activity understanding. *TPAMI*, 2020. 3

[74] Li Liu, Qingle Huang, Sihao Lin, Hongwei Xie, Bing Wang, Xiaojun Chang, and Xiaodan Liang. Exploring inter-channel correlation for diversity-preserved knowledge distillation. In *ICCV*, 2021. 3

[75] Ruiping Liu, Kailun Yang, Alina Roitberg, Jiaming Zhang, Kunyu Peng, Huayao Liu, and Rainer Stiefelhagen. TransSKD: Transformer knowledge distillation for efficient semantic segmentation. *arXiv preprint arXiv:2202.13393*, 2022. 2, 3, 5

[76] Shilong Liu, Lei Zhang, Xiao Yang, Hang Su, and Jun Zhu. Query2label: A simple transformer way to multi-label classification. *arXiv preprint arXiv:2107.10834*, 2021. 3

[77] Ze Liu, Han Hu, Yutong Lin, Zhuliang Yao, Zhenda Xie, Yixuan Wei, Jia Ning, Yue Cao, Zheng Zhang, Li Dong, et al. Swin transformer V2: Scaling up capacity and resolution. In *CVPR*, 2022. 2

[78] Ze Liu, Jia Ning, Yue Cao, Yixuan Wei, Zheng Zhang, Stephen Lin, and Han Hu. Video swin transformer. In *CVPR*, 2022. 2, 6, 7, 14

[79] Ziyu Liu, Hongwen Zhang, Zhenghao Chen, Zhiyong Wang, and Wanli Ouyang. Disentangling and unifying graph convolutions for skeleton-based action recognition. In *CVPR*, 2020. 3

[80] Ilya Loshchilov and Frank Hutter. Decoupled weight decay regularization. *arXiv preprint arXiv:1711.05101*, 2017. 7

[81] Yue Lu, Yujie Wang, and Qian Lu. Effects of exercise on muscle fitness in dialysis patients: A systematic review and meta-analysis. *American Journal of Nephrology*, 2019. 1

[82] Raphael Memmesheimer, Nick Theisen, and Dietrich Paulus. Gimme signals: Discriminative signal encoding for multimodal activity recognition. In *IROS*, 2020. 3

[83] Enrico Maria Minnella, Kenneth Drummond, and Francesco Carli. The impact of prehabilitation on surgical outcomes. *Ann. Esophagus*, 2021. 1

[84] Alessio Monti, Angelo Porrello, Simone Calderara, Pasquale Coscia, Lamberto Ballan, and Rita Cucchiara. How many observations are enough? Knowledge distillation for trajectory forecasting. In *CVPR*, 2022. 2, 5

[85] Arsha Nagrani, Shan Yang, Anurag Arnab, Aren Jansen, Cordelia Schmid, and Chen Sun. Attention bottlenecks for multimodal fusion. In *NeurIPS*, 2021. 7

[86] Theresa H Nakagawa, Érika TU Moriya, Carlos D. Maciel, and Fábio V. Serrão. Trunk, pelvis, hip, and knee kinematics, hip strength, and gluteal muscle activation during a single-leg squat in males and females with and without patellofemoral pain syndrome. *Journal of Orthopaedic & Sports Physical Therapy*, 2012. 4

[87] Daniel Neimark, Omri Bar, Maya Zohar, and Dotan Asselmann. Video transformer network. In *ICCV*, 2021. 2

[88] Linda O'Neill, Annemarie E Bennett, Emer Guinan, John V Reynolds, and Juliette Hussey. Physical recovery in the first six months following oesophago-gastric cancer surgery. identifying rehabilitative needs: a qualitative interview study. *Disability and Rehabilitation*, 2021. 1

[89] Rameswar Panda, Chun-Fu Richard Chen, Quanfu Fan, Ximeng Sun, Kate Saenko, Aude Oliva, and Rogerio Feris. AdaMML: Adaptive multi-modal learning for efficient video recognition. In *ICCV*, 2021. 3

[90] Rameswar Panda, Chun-Fu Richard Chen, Quanfu Fan, Ximeng Sun, Kate Saenko, Aude Oliva, and Rogerio Feris. AdaMML: Adaptive multi-modal learning for efficient video recognition. In *ICCV*, 2021. 3

[91] Mara Paneroni, Carla Simonelli, Manuela Saleri, Laura Bertacchini, Massimo Venturelli, Thierry Troosters, Niccolino Ambrosino, and Michele Vitacca. Muscle strength and physical performance in patients without previous disabilities recovering from COVID-19 pneumonia. *American Journal of Physical Medicine & Rehabilitation*, 2021. 1

[92] Dae Young Park, Moon-Hyun Cha, Daesin Kim, Bohyung Han, et al. Learning student-friendly teacher networks for knowledge distillation. In *NeurIPS*, 2021. 2

[93] Paritosh Parmar and Brendan Tran Morris. What and how well you performed? A multitask learning approach to action quality assessment. In *CVPR*, 2019. 2, 3, 4

[94] Mandela Patrick, Yuki M. Asano, Polina Kuznetsova, Ruth Fong, Joao F. Henriques, Geoffrey Zweig, and Andrea Vedaldi. Multi-modal self-supervision from generalized data transformations. *arXiv preprint arXiv:2003.04298*, 2020. 2

[95] Chenming Peng, Nannan Xi, Zhao Hong, and Juho Hamari. Acceptance of wearable technology: A meta-analysis. In *HICSS*, 2022. 1

[96] Kunyu Peng, Alina Roitberg, Kailun Yang, Jiaming Zhang, and Rainer Stiefelhagen. Delving deep into one-shot skeleton-based action recognition with diverse occlusions. *arXiv preprint arXiv:2202.11423*, 2022. 3, 7

[97] Kunyu Peng, Alina Roitberg, Kailun Yang, Jiaming Zhang, and Rainer Stiefelhagen. Should I take a walk? Estimating energy expenditure from video data. In *CVPRW*, 2022. 2

[98] Cuong Pham, Linh Nguyen, Anh Nguyen, Ngon Nguyen, and Van-Toi Nguyen. Combining skeleton and accelerometer data for human fine-grained activity recognition and abnormal behaviour detection with deep temporal convolutional networks. *MTAP*, 2021. 3

[99] A. J. Piergiovanni, Anelia Angelova, and Michael S. Ryoo. Evolving losses for unsupervised video representation learning. In *CVPR*, 2020. 2

[100] Borislav Radić, Petra Radić, and Din Duraković. Peripheral nerve injury in sports. *Acta Clinica Croatica*, 2018. 1

[101] Nishant Rai, Ehsan Adeli, Kuan-Hui Lee, Adrien Gaidon, and Juan Carlos Niebles. CoCon: Cooperative-contrastive learning. In *CVPR*, 2021. 2

[102] Heilym Ramirez, Sergio A. Velastin, Ignacio Meza, Ernesto Fabregas, Dimitrios Makris, and Gonzalo Farias. Fall detection and activity recognition using human skeleton features. *IEEE Access*, 2021. 1

[103] A. Rasch, A. H. Byström, N. Dalen, N. Martinez-Carranza, and H. E. Berg. Persisting muscle atrophy two years after replacement of the hip. *The Journal of Bone and Joint Surgery. British Volume*, 2009. 1

[104] Tal Ridnik, Gilad Sharir, Avi Ben-Cohen, Emanuel Ben-Baruch, and Asaf Noy. ML-decoder: Scalable and versatile classification head. *arXiv preprint arXiv:2111.12933*, 2021. 3

[105] Alina Roitberg, Kunyu Peng, Zdravko Marinov, Constantin Seibold, David Schneider, and Rainer Stiefelhagen. A comparative analysis of decision-level fusion for multimodal driver behaviour understanding. In *IV*, 2022. 7

[106] David Sanchez-Lorente, Ricard Navarro-Ripoll, Rudith Guzman, Jorge Moises, Elena Gimeno, Marc Boada, and Laureano Molins. Prehabilitation in thoracic surgery. *Journal of Thoracic Disease*, 2018. 1

[107] David Schneider, Saquib Sarfraz, Alina Roitberg, and Rainer Stiefelhagen. Pose-based contrastive learning for domain agnostic activity representations. In *CVPRW*, 2022. 2

[108] Ramprasaath R Selvaraju, Michael Cogswell, Abhishek Das, Ramakrishna Vedantam, Devi Parikh, and Dhruv Batra. Grad-CAM: Visual explanations from deep networks via gradient-based localization. In *ICCV*, 2017. 6, 8, 19

[109] Ayoung Seok and Yongsoon Choi. A study on user experience evaluation of glasses-type wearable device with built-in bone conduction speaker: Focus on the zungle panther. In *TVX*, 2018. 1

[110] Amir Shahroudy, Jun Liu, Tian-Tsong Ng, and Gang Wang. NTU RGB+D: A large scale dataset for 3D human activity analysis. In *CVPR*, 2016. 3

[111] Dian Shao, Yue Zhao, Bo Dai, and Dahua Lin. FineGym: A hierarchical video dataset for fine-grained action understanding. In *CVPR*, 2020. 2, 3

[112] Lei Shi, Yifan Zhang, Jian Cheng, and Hanqing Lu. Two-stream adaptive graph convolutional networks for skeleton-based action recognition. In *CVPR*, 2019. 3

[113] Lei Shi, Yifan Zhang, Jian Cheng, and Hanqing Lu. Skeleton-based action recognition with multi-stream adaptive graph convolutional networks. *TIP*, 2020. 3

[114] Changyong Shu, Yifan Liu, Jianfei Gao, Zheng Yan, and Chunhua Shen. Channel-wise knowledge distillation for dense prediction. In *ICCV*, 2021. 3

[115] Karen Simonyan and Andrew Zisserman. Two-stream convolutional networks for action recognition in videos. In *NeurIPS*, 2014. 2

[116] Jie Song, Ying Chen, Jingwen Ye, and Mingli Song. Spot-adaptive knowledge distillation. *TIP*, 2022. 3

[117] Khurram Soomro, Amir Roshan Zamir, and Mubarak Shah. UCF101: A dataset of 101 human actions classes from videos in the wild. *arXiv preprint arXiv:1212.0402*, 2012. 2, 3, 4, 14

[118] Vladislav Sovrasov. Combining metric learning and attention heads for accurate and efficient multilabel image classification. *arXiv preprint arXiv:2209.06585*, 2022. 3

[119] Sebastian Stein and Stephen J. McKenna. Combining embedded accelerometers with computer vision for recognizing food preparation activities. In *UbiComp*, 2013. 3

[120] Yansong Tang, Zanlin Ni, Jiahuan Zhou, Danyang Zhang, Jiwen Lu, Ying Wu, and Jie Zhou. Uncertainty-aware score distribution learning for action quality assessment. In *CVPR*, 2020. 2, 3

[121] Zhan Tong, Yibing Song, Jue Wang, and Limin Wang. Videomae: Masked autoencoders are data-efficient learners for self-supervised video pre-training. *arXiv preprint arXiv:2203.12602*, 2022. 2

[122] Maurício Cagliari Tosin, Juliano Costa Machado, and Alexandre Balbinot. sEMG-based upper limb movement classifier: Current scenario and upcoming challenges. *JAIR*, 2022. 2

[123] Hugo Touvron, Matthieu Cord, Matthijs Douze, Francisco Massa, Alexandre Sablayrolles, and Hervé Jégou. Training data-efficient image transformers & distillation through attention. In *ICML*, 2021. 2, 5, 7, 8

[124] Du Tran, Lubomir Bourdev, Rob Fergus, Lorenzo Torresani, and Manohar Paluri. Learning spatiotemporal features with 3D convolutional networks. In *ICCV*, 2015. 2

[125] Du Tran, Heng Wang, Lorenzo Torresani, Jamie Ray, Yann LeCun, and Manohar Paluri. A closer look at spatiotemporal convolutions for action recognition. In *CVPR*, 2018. 2

[126] Vo Hoang Trong, Yu Gwang-hyun, Dang Thanh Vu, and Kim Jin-young. Late fusion of multimodal deep neural networks for weeds classification. *Computers and Electronics in Agriculture*, 2020. 2, 5

[127] Roland van den Tillaar, Jens Asmund Brevik Solheim, and Jesper Bencke. Comparison of hamstring muscle activation during high-speed running and various hamstring strengthening exercises. *International Journal of Sports Physical Therapy*, 2017. 4

[128] Ashish Vaswani, Noam Shazeer, Niki Parmar, Jakob Uszkoreit, Llion Jones, Aidan N. Gomez, Łukasz Kaiser, and Illia Polosukhin. Attention is all you need. In *NeurIPS*, 2017. 14

[129] Marina V Viana, Fabio Becce, Olivier Pantet, Sabine Schmidt, Géraldine Bagnoud, John J. Thaden, Gabriella A. M. Ten Have, Mariëlle P. K. J. Engelen, Aline Voidey, Nicolaas E. P. Deutz, and Mette M. Bergera. Impact of β -hydroxy- β - methylbutyrate (HMB) on muscle loss and protein metabolism in critically ill patients: A RCT. *Clinical Nutrition*, 2021. 1

[130] Cheng Wang, Haojin Yang, and Christoph Meinel. Exploring multimodal video representation for action recognition. In *IJCNN*, 2016. 3

[131] Lichen Wang, Zhengming Ding, Zhiqiang Tao, Yunyu Liu, and Yun Fu. Generative multi-view human action recognition. In *ICCV*, 2019. 3

[132] Limin Wang, Yuanjun Xiong, Zhe Wang, Yu Qiao, Dahua Lin, Xiaou Tang, and Luc Van Gool. Temporal segment networks: Towards good practices for deep action recognition. In *ECCV*, 2016. 2

[133] Rui Wang, Dongdong Chen, Zuxuan Wu, Yinpeng Chen, Xiyang Dai, Mengchen Liu, Yu-Gang Jiang, Luowei Zhou, and Lu Yuan. BEVT: BERT pretraining of video transformers. In *CVPR*, 2022. 2

[134] Shiguang Wang, Zhizhong Li, Yue Zhao, Yuanjun Xiong, Limin Wang, and Dahua Lin. Denseflow. <https://github.com/open-mmlab/denseflow>, 2020. 4

[135] Ya Wang, Dongliang He, Fu Li, Xiang Long, Zhichao Zhou, Jinwen Ma, and Shilei Wen. Multi-label classification with label graph superimposing. In *AAAI*, 2020. 3

[136] Ping-Cheng Wei, Kunyu Peng, Alina Roitberg, Kailun Yang, Jiaming Zhang, and Rainer Stiefelhagen. Multi-modal depression estimation based on sub-attentional fusion. *arXiv preprint arXiv:2207.06180*, 2022. 7

[137] Felicity R. Williams, Annalisa Berzigotti, Janet M. Lord, Jennifer C. Lai, and Matthew J. Armstrong. Impact of exercise on physical frailty in patients with chronic liver disease. *Alimentary Pharmacology & Therapeutics*, 2019. 1

[138] Yimeng Wu, Peyman Passban, Mehdi Rezagholizade, and Qun Liu. Why skip if you can combine: A simple knowledge distillation technique for intermediate layers. *arXiv preprint arXiv:2010.03034*, 2020. 3

[139] Fanyi Xiao, Yong Jae Lee, Kristen Grauman, Jitendra Malik, and Christoph Feichtenhofer. Audiovisual slow-fast networks for video recognition. *arXiv preprint arXiv:2001.08740*, 2020. 3

[140] Saining Xie, Chen Sun, Jonathan Huang, Zhuowen Tu, and Kevin Murphy. Rethinking spatiotemporal feature learning: Speed-accuracy trade-offs in video classification. In *ECCV*, 2018. 2

[141] Dezhen Xiong, Daohui Zhang, Xingang Zhao, and Yiwen Zhao. Deep learning for EMG-based human-machine interaction: A review. *IEEE/CAA Journal of Automatica Sinica*, 2021. 2

[142] Jinglin Xu, Yongming Rao, Xumin Yu, Guangyi Chen, Jie Zhou, and Jiwen Lu. FineDiving: A fine-grained dataset for procedure-aware action quality assessment. In *CVPR*, 2022. 2, 3

[143] Lian Xu, Wanli Ouyang, Mohammed Bennamoun, Farid Boussaid, and Dan Xu. Multi-class token transformer for weakly supervised semantic segmentation. In *CVPR*, 2022. 2, 4, 5, 15, 16

[144] Shichao Xu, Yikang Li, Jenhao Hsiao, Chiuman Ho, and Zhu Qi. A dual modality approach for (zero-shot) multi-label classification. *arXiv preprint arXiv:2208.09562*, 2022. 3

[145] Sijie Yan, Yuanjun Xiong, and Dahua Lin. Spatial temporal graph convolutional networks for skeleton-based action recognition. In *AAAI*, 2018. 2, 3, 6, 7, 14

[146] Zhendong Yang, Zhe Li, Mingqi Shao, Dachuan Shi, Zehuan Yuan, and Chun Yuan. Masked generative distillation. *arXiv preprint arXiv:2205.01529*, 2022. 3

[147] Li Yao, Atousa Torabi, Kyunghyun Cho, Nicolas Ballas, Christopher Pal, Hugo Larochelle, and Aaron Courville. Describing videos by exploiting temporal structure. In *ICCV*, 2015. 2

[148] Fanfan Ye, Shiliang Pu, Qiaoyong Zhong, Chao Li, Di Xie, and Huiming Tang. Dynamic GCN: Context-enriched topology learning for skeleton-based action recognition. In *MM*, 2020. 3

[149] Jin Ye, Junjun He, Xiaojiang Peng, Wenhao Wu, and Yu Qiao. Attention-driven dynamic graph convolutional network for multi-label image recognition. In *ECCV*, 2020. 3

[150] Renchun You, Zhiyao Guo, Lei Cui, Xiang Long, Yingze Bao, and Shilei Wen. Cross-modality attention with semantic graph embedding for multi-label classification. In *AAAI*, 2020. 3

[151] Pengfei Zhang, Cuiling Lan, Wenjun Zeng, Junliang Xing, Jianru Xue, and Nanning Zheng. Semantics-guided neural networks for efficient skeleton-based human action recognition. In *CVPR*, 2020. 3

[152] Zhengbo Zhang, Chunluan Zhou, and Zhigang Tu. Distilling inter-class distance for semantic segmentation. In *IJCAI*, 2022. 3

[153] Borui Zhao, Quan Cui, Renjie Song, Yiyu Qiu, and Jiajun Liang. Decoupled knowledge distillation. In *CVPR*, 2022. 3

[154] Hang Zhao, Zhicheng Yan, Lorenzo Torresani, and Antonio Torralba. HACS: Human action clips and segments dataset for recognition and temporal localization. In *ICCV*, 2019. 3

[155] Jiaojiao Zhao, Xinyu Li, Chunhui Liu, Shuai Bing, Hao Chen, Cees G. M. Snoek, and Joseph Tighe. Tuber: Tuber-transformer for action detection. In *CVPR*, 2022. 2

[156] Jiawei Zhao, Ke Yan, Yifan Zhao, Xiaowei Guo, Feiyue Huang, and Jia Li. Transformer-based dual relation graph for multi-label image recognition. In *ICCV*, 2021. 3

[157] Bolei Zhou, Alex Andonian, Aude Oliva, and Antonio Torralba. Temporal relational reasoning in videos. In *ECCV*, 2018. 2

[158] Yi Zhu, Zhenzhong Lan, Shawn Newsam, and Alexander Hauptmann. Hidden two-stream convolutional networks for action recognition. In *ACCV*, 2018. 2

[159] Yichen Zhu and Yi Wang. Student customized knowledge distillation: Bridging the gap between student and teacher. In *ICCV*, 2021. 3

[160] Han Zou, Jianfei Yang, Hari Prasanna Das, Huihan Liu, Yuxun Zhou, and Costas J. Spanos. WiFi and vision multimodal learning for accurate and robust device-free human activity recognition. In *CVPRW*, 2019. 3

[161] Qin Zou, Yanling Wang, Qian Wang, Yi Zhao, and Qingquan Li. Deep learning-based gait recognition using smartphones in the wild. *TIFS*, 2020. 3

A. Discussion of Societal Impacts and Limitation

Societal Impacts. In our work, a new dataset targeting at the AMGE is collected based on YouTube videos, termed as MuscleMap136. We further extend the existing famous activity recognition dataset, UCF101 [117] and HMDB51 [67], with AMGE annotations, which are termed as Muscle-UCF90 and Muscle-HMDB41. We build up MuscleMap benchmark for the AMGE by using statistic baselines and existing activity recognition approaches

including both video-based and skeleton-based methods, while the three aforementioned datasets are all considered. Through the experiments we find that the generalizability targeting AMGE on unseen activities is not satisfied for the existing activity recognition approaches. In order to tackle this issue, we propose a new cross-modality knowledge distillation approach named as TRANSM^3E while using MViTv2-S [72] as its basic backbone. The proposed approach alleviates the generalization problem in a certain degree, however there is still large space for further improvement and future research. The AMGE performance gap between the seen activities and unseen activities illustrates that our model has potential to give offensive predictions, misclassifications and biased content which may cause false prediction resulting in the negative social impact. The dataset and code will be released publicly.

Limitations. The annotations of MuscleMap136 are created for each video clip instead of being created for each frame and the label is binary without giving the different levels of muscle activations. In addition, there is still a clear gap between the performance of seen and unseen categories. While our method has enhanced the generalization capacity, there remains room for future improvement.

B. Baseline Introduction

Video-based approaches (*i.e.*, I3D [18], SlowFast [42] and MViTv2 [72, 39]), skeleton-based approaches (*i.e.*, ST-GCN [145], CTR-GCN [20] and HD-GCN [69]), and statistic calculations (*i.e.*, randomly guess) are selected to serve as baselines to formulate our AMGE benchmark on the mentioned three datasets. Statistic baselines serve to provide the borderline to verify whether the performance of a deep learning model is better than that of the random guess or a fixed prediction. Skeleton-based approaches are selected since they directly take geometric relationship of the human body into consideration without the disruption from the background. Regarding video-based approaches, transformer-based models, *i.e.*, MViTv2 [72] and VideoSwin [78], and convolutional neural network (CNN)-based models, *i.e.*, C2D [43], I3D [18], Slow [42] and Slow-Fast [42], are leveraged due to their good performance while handling the activity recognition task. Transformers are expected to have better performance compared with CNNs due to its excellent long-term reasoning ability [128], which also show superior performance for AMGE on the leveraged three datasets.

C. More Ablation Studies of TransM^3E

In this section, we provide more ablation studies on our TRANSM^3E approach. In Section C.1 more details and clarifications regarding our ablation study for the MCTKD component are illustrated. In Section C.2 we conduct exper-

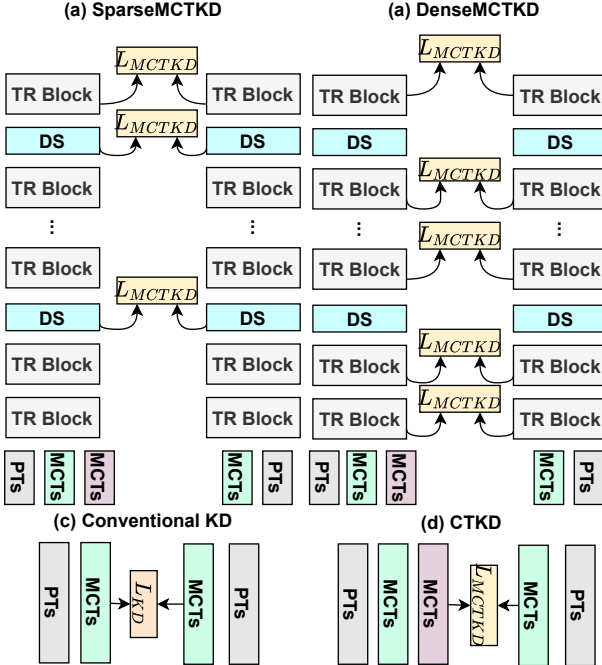


Figure 6: An overview of the details regarding our ablation study for the MCTKD position and format, where (a) we execute MCTKD after the downsampling of the pooling layer and after the final transformer block to formulate SparseMCTKD, (b) we leverage the MCTKD after each transformer block (TR Block) to formulate the DenseMCTKD, (c) indicates the conventional KD (KD directly on the MCTs between main modality and auxiliary modality), (d) indicates the MCTKD we leveraged.

iments to illustrate the superiority of our proposed MCTs compared with MCT proposed from [143]. In Section C.3, the ablation regarding the size of MCTs is shown. In Section C.4, we introduced the performance of different attention formats leveraged to formulate the MCTF. In Section C.5, the ablation regarding the number of heads while constructing MCTF for the attention calculation is introduced. In Section C.6, we make comparison among different combinations regarding modalities for the TRANSM³E approach. In Section C.7, we introduce the ablation regarding the percentage of KD for MCTKD.

C.1. More details of the ablation of MCTKD

Since we introduced the ablation regarding MCTKD in our main paper with experimental results, only more details regarding the KD format and position will be introduced in this section. In order to make it clearer for understanding, we illustrate more details regarding the KD/MCTKD position in Figure 6 to give a detailed clarification. For the MCTKD related approaches, we use the MCTKD as depicted by (d), where the KD is executed between the knowledge receiver MCTs of the main modality and the sender

MCTs of the auxiliary modality. For all the other basic KD-based approaches, we use the format as depicted by (c), where the KD is executed between the MCTs of the main modality and the MCTs of the auxiliary modality, regarded as conventional KD. All the experiments are executed with MCTs while without MCTF aggregation. We simply average the MCTs for all the experiments in this ablation. Regarding the Sparse format as depicted in (a), the knowledge of the auxiliary modality is only transferred after the size reduction of the pooling layer denoted as Down-sampling (DS) in Figure 6 and after the final layer. Only SparseMCTKD and DenseMCTKD are depicted since the SparseKD and DenseKD use the same position settings. SparseKD/MCTKD aims at reducing the KD/MCTKD calculation by selecting the most important intermediate layers to transfer the knowledge. After each pooling layer which has size reduction, the informative clues will be highlighted after the pooling, which makes the corresponding changes of the tokens from auxiliary modality necessary to be integrated through KD/MCTKD. In this case we choose the position after the pooling with size reduction to do the KD/MCTKD on the intermediate layer. DenseKD/MCTKD is designed to transfer the knowledge directly after each transformer block in order to leverage the knowledge from the other modality thoroughly. We make use of both KD positions to conduct comparison and select the most appropriate method to build the MCTKD in our final model.

C.2. Comparison between MCTs and MCT

Comparison experiments among MViT2-S [72], MViT2-S + MCT [143] and MViT2-S +MCTs (our approach with only MCTs) on the MuscleMap136 dataset are introduced in Table 8. The MCT from Xu *et al.* [143] has clear class assignment at the final score prediction achieved through averaging the N_C classification (cls) tokens along channel dimension, resulting a 1-channel output for each category. For our proposed MCTs, instead of using clear class assignment for the cls tokens for the supervision and prediction, we leverage unclear class assignment achieved through averaging the N_C cls tokens along token dimension, projecting the averaged tokens into N_C channels and then using a Softmax layer to obtain the final prediction. The unclear class assignment allows a mixture of the underlying cues for AMGE in the intermediate feature level which is verified to have strong capability for the improvement regarding the generalizability, as shown in Table 8. The MCT proposed from Xu [143] could not address the AMGE well since it is originally designed for semantic segmentation, which is much far away from the AMGE task. Compared with the MViT2-S baseline, MViT2-S + MCT [143] has large performance decrease while our proposed MCTs help to improve the performance either on the seen activities or on the unseen activities during the test and evaluation,

Table 8: Comparison between MCT from [143] and our MCTs.

Method	Val.s	Val.u	Val.a	Test.s	Test.u	Test.a
MViTv2-S	98.5	55.0	77.0	98.5	55.5	77.2
MViTv2-S + MCT [143]	93.8	45.7	69.8	95.5	44.4	70.0
Ours (Wth only MCTs)	98.7	58.3	78.5	98.8	61.3	80.1

which illustrates the superiority regarding the design of the unclear class alignment mechanism in our MCTs targeting AMGE task specifically.

C.3. Ablation of the token size of the MCTs

In order to find out the proper size of the MCTs for the AMGE task, we have done the corresponding ablation study in the Table 9. During the ablation of the number of the cls tokens, we find that when the token number of MCTs matches the number of the prediction class, TRANSM³E harvests the best performance especially targeting the unseen activities. Thereby the cls token size in our TRANSM³E is set as 20 which is the same with the class size for AMGE task and all the experiments in the main context of our work use 20 as the MCTs size. The experiments are done for TRANSM³E without MCTF.

C.4. Ablation of the diverse attention components of MCTF

According to the introduction of the main text, we have three different attentions to integrate the features from the KD receiver MCTs to the original MCTs used for classification for both the major modality and the auxiliary modality, *e.g.*, \mathbf{A}_{mm}^m , \mathbf{A}_{mr}^m , \mathbf{A}_{rm}^m , \mathbf{A}_{rr}^r , \mathbf{A}_{mr}^r and \mathbf{A}_{rm}^r . We conduct the comparison among using only self-attention (case 1), *e.g.*, using only \mathbf{A}_{mm}^m and \mathbf{A}_{rr}^r , using only \mathbf{A}_{mr}^m and \mathbf{A}_{rm}^m (case 2) by taking major modality as Query, using only \mathbf{A}_{mm}^m and \mathbf{A}_{rm}^r (case 3) while leveraging the auxiliary modality as the Query, using \mathbf{A}_{mm}^m , \mathbf{A}_{rr}^r , \mathbf{A}_{mr}^m and \mathbf{A}_{mr}^r (case 4), using \mathbf{A}_{mm}^m , \mathbf{A}_{rr}^r , \mathbf{A}_{rm}^m and \mathbf{A}_{rm}^r (case 5), using \mathbf{A}_{mr}^m , \mathbf{A}_{rm}^m , \mathbf{A}_{mr}^r and \mathbf{A}_{rm}^r (case 6) and using all (case 7). Through the comparison we find that using all attentions (case 7) shows the best performance with mAP 99.0% and 60.6% for the val.s and val.u and mAP 99.0% and 63.4% for the test.s and test.u. Thereby the case 7 is leveraged to construct our TRANSM³E approach. All the experiments are done by using TRANSM³E-SMALL.

C.5. Ablation of the head number of MCTF

Since MCTF is transformer-based fusion architecture between the Receiver MCTs from the main modality and original MCTs from the main modality, the number of heads used in the attention generation has potential to deliver an influence for the AMGE performance regarding the TRANSM³E approach. Thereby, we conduct ablations regarding the number of head in Table 10 for the pro-

Table 9: Ablation for the token size of MCTs on the MuscleMap136 dataset.

MCTSize	Val.s	Val.u	Val.a	Test.s	Test.u	Test.a
1	98.5	55.0	77.0	98.8	55.5	77.2
5	98.7	54.0	76.4	98.9	53.6	76.3
10	98.4	54.4	76.4	98.9	54.4	76.7
15	98.6	53.4	76.0	99.0	53.5	76.3
20	98.7	60.5	79.6	98.8	61.3	80.1
25	98.5	55.3	76.9	99.3	55.5	77.4
30	98.4	54.2	76.3	98.8	55.1	77.0

Table 10: Ablation regarding the number of head for TRANSM³E on the MuscleMap136 dataset.

HeadNum	Val.s	Val.u	Val.a	Test.s	Test.u	Test.a
1	99.0	60.6	79.8	99.0	63.4	81.2
2	98.8	60.2	79.5	98.9	62.9	80.9
3	99.0	60.1	79.6	98.9	63.2	81.1
4	98.8	60.3	79.6	99.0	62.8	80.9
5	99.0	60.0	79.5	99.1	62.9	81.0

Table 11: Ablation regarding the attention combination for TRANSM³E on the MuscleMap136 dataset.

AttCaseNum	Val.s	Val.u	Val.a	Test.s	Test.u	Test.a
1	98.9	59.9	79.4	98.9	62.2	80.6
2	99.0	59.4	79.2	98.9	62.2	80.6
3	98.7	59.8	79.3	99.0	62.9	81.0
4	98.8	59.6	79.2	99.0	62.5	80.8
5	98.8	60.2	79.5	98.9	62.4	80.7
6	98.9	60.2	79.6	99.0	63.2	81.1
7	99.0	60.6	79.8	99.0	63.4	81.2

posed MCTF to search for the best setting. Through the comparison, MCTF with head number 1 achieves the best performance compared with all other settings. We also use head number 1 in the MCTF to get the best model for TRANSM³E. All the experiments are done by using TRANSM³E-SMALL.

C.6. Ablation studies about using other modalities in TRANSM³E

The major and auxiliary modalities are chosen as RGB and RGB Diff according to the performance of different modality as mentioned in our main paper. However, it is still interesting to see if TRANSM³E helps for the performance improvement when other modalities are leveraged. In order to investigate this concern we conduct ablation experiments in Table 12 regarding RGB+RGB Diff, RGB+OPT (optical flow), RGB Diff + OPT, respectively. The performance of TRANSM³E using RGB+OPT also shows competitive results which achieves second best performance on the MuscleMap136, illustrating that TRANSM³E can generalize to other modality settings while delivering a competitive results. The performance of RGB Diff+OPT is unsatisfied compared with the other two settings, which showcases that the proposed approach needs an informative modality serving as the major modality.

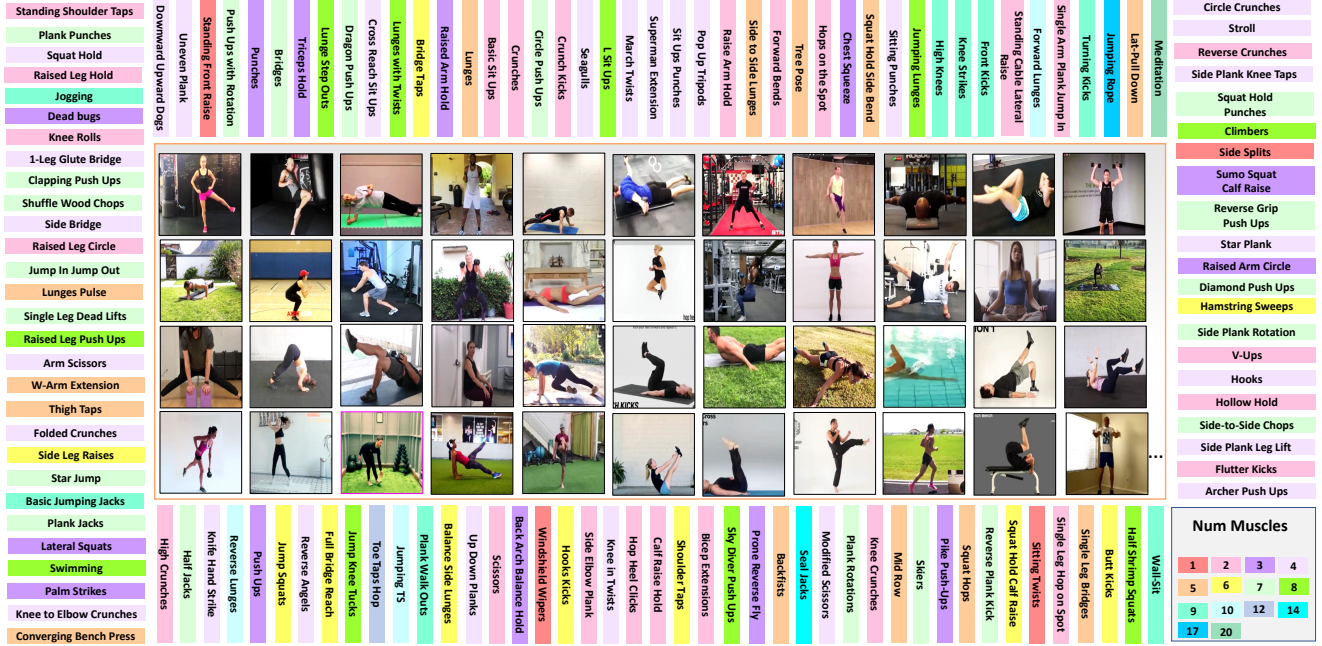


Figure 7: An overview of MuscleMap136 dataset. In the center there are some samples coming from different activities. The legends outside denote the 136 activities included by the MuscleMap136 dataset. On the right bottom corner, the illustration for each color is given regarding how many muscles are activated for each activity.

Table 12: Ablation regarding the fusion of different modality.

AttCaseNum	Val_s	Val_u	Val_a	Test_s	Test_u	Test_a
RGB+RGB DIFF	99.0	60.6	79.8	99.0	63.4	81.2
RGB+OPT	98.6	60.4	62.4	98.7	63.2	81.0
RGB DIFF+OPT	96.2	58.7	60.7	96.9	56.6	76.8

C.7. Ablation of the percentage of the auxiliary modality for MCTKD

We build our architecture based on [42, 72]. During the data augmentation procedure, the input video will be sampled into two clips by using random start index with a fixed stride. If we use $v_{1,m}$ and $v_{2,m}$ to denote the two clips from the major modality, the corresponding RGB Diff for each clip is termed as $v_{1,r}$ and $v_{2,r}$, which are calculated based on a fixed temporal stride for each frame. During our experiments, we find that if we execute the MCTKD between $v_{1,m}$ and $v_{2,r}$, while making the $v_{1,r}$ as zero tensor and doing MCTKD between $v_{2,m}$ and the zeroed $v_{1,r}$ (MCTKD percentage: 50%, case 3), it will achieve the best performance as shown in Table 13. This setting is thereby leveraged to formulate our best model. We also conduct ablation experiments among case 1 (where MCTKD between $v_{1,m}$ and $v_{1,r}$ and MCTKD between $v_{2,r}$ and $v_{2,m}$ are leveraged), case 2 (where MCTKD between $v_{1,r}$ and $v_{1,m}$ and MCTKD between $v_{2,m}$ and $v_{2,r}$ are leveraged), case 3 as aforementioned, and case 4 (where MCTKD between $v_{1,m}$ and zero tensor and MCTKD between $v_{2,m}$ and zero tensor are leveraged).

Table 13: Ablation regarding the percentage of distilled knowledge for MCTKD approach.

Experiments	Val_s	Val_u	Val_a	Test_s	Test_u	Test_a
case 1	99.0	60.5	79.8	99.0	62.8	80.9
case 2	99.0	60.4	79.7	99.0	63.0	81.0
case 3	99.0	60.6	79.8	99.0	63.4	81.2
case 4	99.0	60.1	79.6	99.0	62.6	80.8

Table 14: Comparison between end-to-end AMGE approaches and the lookup table with HAR.

Method	Val_s	Val_u	Val_a	Test_s	Test_u	Test_a
HAR Lookup	95.4	38.8	67.1	95.7	38.0	66.9
MViTv2	98.5	55.0	77.0	98.8	55.5	77.2
Ours	99.0	60.6	79.8	99.0	63.4	81.2

C.8. Clarification regarding the relationship between HAR and AMGE

To investigate the relation between AMGE and HAR, we conduct comparison between end-to-end AMGE and HAR-based method, *i.e.*, HAR + lookup table. As shown in Table 14, we found that AMGE cannot be well addressed by using HAR + lookup table. The performance of HAR-based approach has a comparable performance for seen activities, however the performance on unseen activities is low, showing the shortcoming that this approach cannot generalize to the unseen activities with only 38.8% and 38.0% in mAP on val_u and test_u, while end-to-end approaches surpass it obviously on the unseen activities. HARL is trained using MViTv2-S (ImageNet1K pretrained) supervised by action labels while using lookup tables to get

AMGE. Unseen actions are classified as one of the seen action classes and the muscle activations of this known class is assigned to that unseen action. Tab. 14 shows that AMGE models learn AMGE based on generalizable body movements beyond learning discrete actions in lookup relationship. TRANSM³E shows significantly better generalization ability compared to HARL, indicating the output space of AMGE models is not limited by the seen actions. Tab. 8 addresses the concern of a limited output space. Compared with baselines, our model’s improvement on test/val_u shows the AMGE generalizability can be improved, verifying generalizable AMGE is achievable under limited actions.

C.9. Analysis regarding why ST-GCN has better performance than CTR-GCN

As AMGE is a different task compared to HAR, AMGE aims for a better understanding of muscle contributions (MC). The experiments showed the cross-task generalization ability of CTR-GCN is insufficient. Its channel specific correlation separates joints into groups while AMGE requires knowledge on the MC of the whole body. CTR-GCN’s joint clustering can narrow the analysis scope into a local view while AMGE requires a global analysis.

D. Details of the Benchmark and Implementation

In this section we will introduce more details regarding the proposed MuscleMap136 dataset and the other two annotation sets together with more implementation details. We first demonstrate more details regarding the annotation for the AMGE Section D.1. The evaluation protocol and the metric are introduced in Section D.2. More implementation details are introduced in Section D.3.

D.1. Details of the AMGE annotation.

The AMGE annotation for each activity type is achieved by searching which muscles are leveraged during the specific kind of activity. Assuming for activity X we can find N_X online websites resources, describing the major activation regions of the human muscles. The example online resource link is not included here in order to maintain anonymous submission since the website link is not recommended to be provided in the author guideline and it is not possible to check if the website has tracking of the visitor or not. There is possible to obtain annotation disagreement among different websites. Considering this case we set up the acceptance threshold for each occurred muscle region as $N_T = \text{int}(N_X/2)$. If a certain region of muscles occurs $\geq N_T$, this region is annotated as True to construct our AMGE annotation. In this manner, we annotate the activity-specific video clip in multi-label manner to formulate our MuscleMap benchmark. The number of activated

muscles for each activity in the MuscleMap136 dataset is depicted by different color marked at the right bottom corner of Figure 7. Finally we annotate the commonly leveraged human body muscles in the daily life into 20 muscle regions, *i.e.*, *neck and head region*, *chest region*, *shoulder region*, *biceps region*, *triceps region*, *forearms region*, *upper back region*, *latissimus region*, *obliques region*, *upper abdominis region*, *lower abdominis region*, *lower back region*, *hamstring region*, *quadriceps region*, *calves region*, *inner thigh region*, *outer thigh region*, *gluteus region*, *feet ankles region*, and *wrists region*. We rearrange *occipitofrontalis*, *temporoparietalis*, *levator labii superioris*, *masticatorii*, *sternocleidomastoideus* as *neck and head muscle region*; *pectoralis major* as *chest region*; *deltoides* as *shoulder region*; *biceps brachii* as *biceps region*; *triceps brachii* as *triceps region*; *flexor carpi radialis*, *palmaris longus*, *abductor pollicis longus* as *forearm region*; *trapezius* as *upper back region*; *latissimus dorsi* as *latissimus region*; *external oblique*, *serratus anterior* as *obliques region*; *rectus abdominis*, *quadratus lumborum* as *upper abdominis region*; *transversus abdominis*, *pyramidalis* as *lower abdominis region*; *erector spinae* as *lower back region*; *biceps femoris*, *semimembranosus*, *semitendinosus* as *hamstring region*; *rectus femoris*, *vastus medialis* as *quadriceps region*; *gastrocnemius*, *soleus* as *calves region*; *adductor longus*, *sartorius*, *gracilis* as *inner thigh region*; *iliotibial tract* as *outer thigh region*; *gluteus maximus* as *gluteus region*; *peroneus longus and brevis*, *extensor digitorum longus*, *flexor hallucis longus*, *flexor digitorum longus*, *peroneus tertius*, *tibialis posterior* as *feet ankles region*; *extensor pollicis*, *1st dorsal interosseous*, *pronator quadratus* as *wrists region*.

D.2. Details of the evaluation protocol and metric

Evaluation protocol. In order to well evaluate the generalizability of the leveraged approaches for AMGE task, we formulate the unseen evaluation/test and seen evaluation/test simultaneously. For MuscleMap136, 20 of 136 activities are leverage to formulate the unseen test and evaluation set, which are *hollow hold*, *v-ups*, *calf raise hold*, *modified scissors*, *scissors*, *reverse crunches*, *march twists*, *hops on the spot*, *up and down planks*, *diamond push ups*, *running*, *plank jacks*, *archer push ups*, *front kicks*, *triceps dip hold*, *side plank rotation*, *raised leg push ups*, *reverse plank kicks*, *circle push ups*, *shoulder taps*. The activity types of our proposed MuscleMap136 dataset and some samples from different activities are depicted in Figure 7. The sample number for train, val_u, val_s, test_u, test_s sets are 8, 837, 1, 611, 1, 473, 1, 612 and 1, 474. The performances are finally averaged for unseen and seen sets (test_a and val_a). For Muscle-UCF90 and Muscle-HMDB41, 9 of 90 (*hammering*, *shaving beard*, *knitting*, *shot put*, *diving*, *bowling*, *skiing*, *pole vault*, *salsa spin*) and 6 of 41 (*push*,

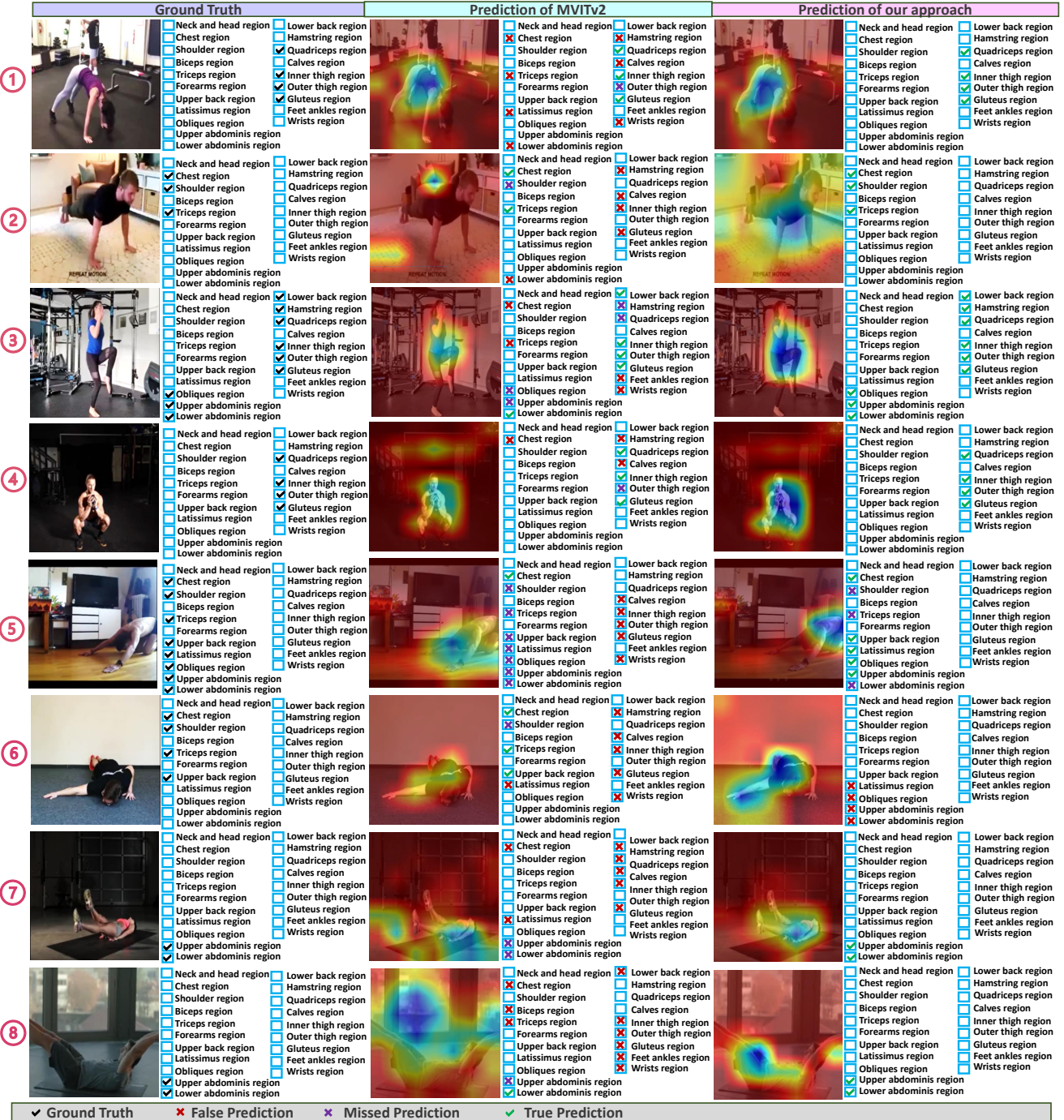


Figure 8: An overview of the qualitative experimental results for MViTv2-S [72] baseline and TRANS^M³E-SMALL. Grad-Cam [108] visualization considering the gradients of the first normalization layer of the last transformer block is given for each method and for each sample, where the cold color region is focused. The ground truth of the selected sample is on the left column, the prediction and gradients visualization of the MViTv2-S and our approach are separately shown in the middle and on the right hand sides together with their predictions.

kick, shoot gun, catch, turn, stand) activities are chosen to formulate the unseen test and evaluation sets, respectively.

We randomly pickup half of each unseen activity to construct the unseen evaluation set and the rest is leveraged to

construct the unseen test set. After the training of the leveraged model, we test the performance of the trained model on seen/unseen evaluation and seen/unseen test sets, and then average the performance of seen and unseen sets to get the averaged performance on evaluation and test sets by considering both seen and unseen activities which are both important for the AMGE task. For Muscle-HMDB41, the sample number for train, val_u, val_s, test_u, test_s sets are 3,311, 552, 422, 552 and 423. For Muscle-UCF90, the sample number for train, val_u, val_s, test_u, test_s sets are 7,151, 1,192, 509, 1,192 and 509. The dataset, protocols and the instruction regarding the evaluation will be publicly released.

Evaluation metric. Mean averaged precision (mAP) is used as the evaluation metric as mentioned in our main paper. Assuming that $l_i, i \in 1, N_{test_u}$ is the multi-hot annotation for the sample i in the test_u set and $Preds_i, i \in 1, N_{test_u}$ is the prediction of the model for the given sample i, we first concatenate the labels to get the label vector L . We first select the subset of the concatenated list of $Preds$ and L by calculate the mask through $m = (L == 1)$. The corresponding subsets are thereby denoted as $Preds[m]$ and $L[m]$. Then we calculated the mean averaged precision score using the existing function from sklearn [13]. We further give more qualitative experimental results in Figure 8 for the GradCam Visualization of the gradients of the first normalization layer of the last transformer block. Through the comparison with the MViT-S baseline we could find that our approach has more concentrated focus on the correct activated region, demonstrating the superiority of the proposed several mechanisms regarding the understanding of the video- based AMGE. This evaluation protocol follows the multi-label classification protocol according to the repository of PySlowFast [42].

D.3. Further implementation details

We further illustrate more implementation details apart from what has been mentioned in our main paper. The input video for train, test and val is center cropped and rescaled as 224x224 with color jitter parameter as 0.4. For our TRANSM³E-SMALL, we use 16 MViT-S blocks and choose the number of head as 1. The feature dimension of the patch embedding net is 96 while using 3D CNN and choosing the patch kernel as {3, 7, 7}, patch stride kernel as {2, 4, 4} and patch padding as {1, 3, 3}. The MLP ratio for the feature extraction block is 4.0, QKV bias is chosen as True and the path dropout rate is chosen as 0.2. The dimension of the tokens and number of heads are multiplied with 2 after the 1-th, 3-th, and 14-th blocks. The pooling kernel of QKV is chosen as {3, 3, 3}, the adaptive pooling stride of KV is chosen as {1, 8, 8} while the stride for the pooling on Q is chosen as {1, 2, 2} for the 1-th, 3-th and 14-th block. For the rest blocks among 0-15 th blocks,

the stride for the pooling on Q is chosen as {1, 1, 1}. Regarding the MCTF, we choose head number as 1, the QK scale number as 0.8, the dropout for attention as 0.0 and the dropout rate of the path as 0.2. The input embeddings of the MCTF has 768 channels while the intermediate embeddings of the MCTF structure has the same number of channel with the input of MCTF. For the TRANSM³E-BASE, the major difference is the number of block which is changed into 24. The pooling kernel of QKV is chosen as {3, 3, 3}, the adaptive pooling stride of KV is chosen as {1, 8, 8} and the stride for the pooling on Q is chosen as {1, 2, 2} for the 2-th, 5-th and 21-th block. For the rest blocks among 0-23 th blocks, the stride for the pooling on Q is chosen as {1, 1, 1}. Regarding the qualitative results as shown in Figure 8 and the qualitative results shown in our main paper, we choose 0.05 as the threshold for the acceptance as a true prediction for each muscle class.